

Journal of Materials Chemistry C

Accepted Manuscript



This is an *Accepted Manuscript*, which has been through the Royal Society of Chemistry peer review process and has been accepted for publication.

Accepted Manuscripts are published online shortly after acceptance, before technical editing, formatting and proof reading. Using this free service, authors can make their results available to the community, in citable form, before we publish the edited article. We will replace this *Accepted Manuscript* with the edited and formatted *Advance Article* as soon as it is available.

You can find more information about *Accepted Manuscripts* in the [Information for Authors](#).

Please note that technical editing may introduce minor changes to the text and/or graphics, which may alter content. The journal's standard [Terms & Conditions](#) and the [Ethical guidelines](#) still apply. In no event shall the Royal Society of Chemistry be held responsible for any errors or omissions in this *Accepted Manuscript* or any consequences arising from the use of any information it contains.



ARTICLE

Photophysical and electroluminescent properties of bis(2',6'-difluoro-2,3'-bipyridinato-N,C4')iridium(picolate) complexes: Effect of electron-withdrawing and electron-donating group substituent at the 4' position on the pyridyl moiety of the cyclometalated ligand

Received 00th January 20xx,
Accepted 00th January 20xx

DOI: 10.1039/x0xx00000x

www.rsc.org/

K. S. Bejoymohandas,^{a, b} Arunandan Kumar,^c S. Varughese,^a E. Varathan,^d V. Subramanian^d and M. L. P. Reddy*^{a, b}

Herein, we have synthesized a series of 2',6'-difluoro-2,3'-bipyridine cyclometalating ligands by substituting electron-withdrawing (–CHO, –CF₃, –CN) and electron-donating (–OMe, –NMe₂) groups at the 4' position of the pyridyl moiety and utilized for the construction of five new iridium(III) complexes (**Ir1–Ir5**) in the presence of picolate as an ancillary ligand. The photophysical properties of the developed iridium(III) compounds were investigated with a view to understand the substituent effects. The strong electron-withdrawing (–CN) group containing iridium(III) compound (**Ir3**) exhibits highly efficient genuine green phosphorescence ($\lambda_{\text{max}} = 508$ nm) at room temperature in solution and in thin film, with an excellent quantum efficiency (Φ_{PL}) of 0.90 and 0.98, respectively. On the other hand, the –CF₃ group substituted iridium(III) compound (**Ir2**) displays a sky-blue emission ($\lambda_{\text{max}} = 468$ nm) with a promising quantum efficiency ($\Phi_{\text{PL}} = 0.88$ and 0.84 in solution and in thin film, respectively). The –CHO substituted iridium(III) complex (**Ir1**) showed greenish-yellow emission ($\lambda_{\text{max}} = 542$ nm). Most importantly, the strong electron-donating –NMe₂ substituted iridium(III) complex (**Ir5**) gives a structureless and a broad emission profile in the wavelength region 450 to 700 nm ($\lambda_{\text{max}} = 520$ nm) with a poor quantum efficiency. An intense blue phosphorescence with impressive quantum efficiency, especially in thin-film noted in the case of –OMe substituted iridium(III) complex (**Ir4**). Comprehensive density functional theory (DFT) and time-dependent DFT (TD-DFT) approaches have been performed on the ground and excited states of the synthesized iridium(III) complexes, in order to obtain information about the absorption and emission processes and to gain deeper insights into the photophysical properties. The combinations of a smaller $\Delta E_{\text{S}_1-\text{T}_1}$ and higher contribution of ³MLCT in the emission process result in the higher quantum yields and lifetime values for complexes **Ir1–Ir3**. Multi-layered Phosphorescence Organic Light Emitting Diodes (PhOLEDs) were designed using the phosphorescent dopants **Ir2**, **Ir3** and **Ir4** and evaluated their electroluminescence properties. The compound **Ir4** at a doping level of 5 wt% shows the best performance with an external quantum efficiency of 4.7%, in nonoptimized device, and power efficiency of 5.8 lm W⁻¹, together with a true-blue chromacity $\text{CIE}_{x,y} = 0.15, 0.17$ recorded at maximum brightness of 33,180 cd/m².

Introduction

Cyclometalated iridium(III) complexes are frequently

considered as the most promising family of triplet emitters for potential applications in Phosphorescence Organic Light Emitting Diodes (PhOLEDs).^{1–26} This is essentially due to their excellent phosphorescent quantum efficiencies, short lifetime of triplet excited states, flexibility in colour tuning and thermal and electrochemical stability.^{27–44} In particular, phosphorescent emitting compounds based on iridium(III) phenylpyridine derivatives have drawn attention and being successfully applied in PhOLED fabrications because they are efficient phosphorescent materials emitting light in the regions of blue, green and red.^{28,45–51} Accordingly, several groups have demonstrated that phosphorescence emission wavelengths can be tuned in the blue to red region by functionalization on the phenyl moiety of 2-phenylpyridine of iridium(III) complexes with electron-withdrawing and electron-donating substituents.^{52–67} However, there are some genuine difficulties

^a Materials Science and Technology Division, CSIR-Network of Institutes for Solar Energy, CSIR-National Institute for Interdisciplinary Science & Technology (CSIR-NIIST), Thiruvananthapuram-695 019, India. E-mail: mlpreddy55@gmail.com

^b Academy of Scientific and Innovative Research (AcSIR), New Delhi 110025, India.

^c Laboratoire Interdisciplinaire Carnot de Bourgogne (ICB) UMR 6303 CNRS, Université de Bourgogne, 9, Av. Savary, BP 47870, 21078 Dijon Cedex, France.

^d Chemical Laboratory, CSIR-Central Leather Research Institute, Chennai – 600 020, India.

†Electronic Supplementary Information (ESI) available: X-ray crystallographic data in CIF format for the complexes **Ir2** and **Ir4** [CCDC 973778 (**Ir2**) and 1005716 (**Ir4**)], NMR and MASS spectra of ligands and complexes, TGA–DSC thermal curves, cyclic voltammograms, lifetime curves, selected bond lengths and angles, intermolecular interactions, calculated transitions of **Ir1–Ir5** in CH₂Cl₂ media and composition of the MOs and the assignment of different fragments. CIF files. See DOI: 10.1039/x0xx00000x

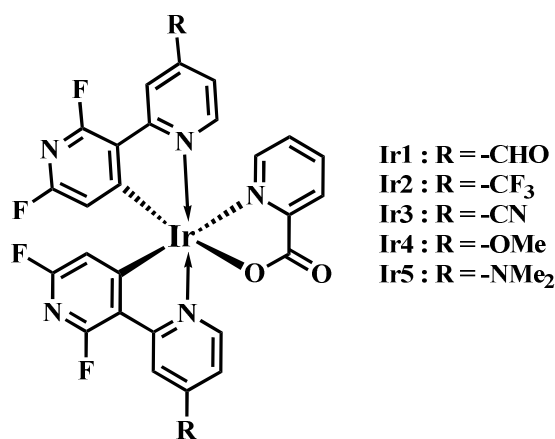
in the development of blue phosphorescent complexes with respect to chromaticity, emission efficiency and stability of the material, as compared with green and red phosphorescent complexes.^{23,68-74}

In order to overcome some of the difficulties in developing a robust blue emitter, Lee *et al.*⁷⁵ have introduced a new type of *fac*-iridium(III) complex containing fluorinated bipyridine as a cyclometalated ligand and investigated the photophysical properties. The emission maximum of *fac*-tris(2',6'-difluoro-2,3'-bipyridinato-N,C4')iridium(III) complex at room temperature has been reported as 438 nm with a high quantum efficiency ($\Phi_{\text{PL}} = 0.71$). However, it has a very low-lying HOMO energy (*ca.* 6.4 - 6.5 eV), making it difficult to find suitable host in the PhOLED applications. In the subsequent studies, Kang and co-workers⁷⁶ have addressed these limitations by replacing one of the dfppy ligands with an appropriate ancillary ligand such as 2-picolinate, acetylacetonate or dipivolylmethonate to elevate the HOMO energy of Ir(dfppy)₃ compound, so that it matches well with that of common host molecule such as 4,4'-N,N'-dicarbazolebiphenyl (CBP). To prevent detrimental aggregation phenomena, Yang *et al.*⁷⁷ have introduced a bulky *tert*-butyl group in the 4' position of the pyridyl moiety of 2',6'-difluoro-2,3'-bipyridine and constructed a series of heteroleptic iridium(III) complexes in the presence of pyridyl-azole as an ancillary ligand and investigated their photophysical properties. These complexes displayed intense phosphorescent blue emission ($\lambda_{\text{em}} = 440$ nm) at room temperature in solution and in thin film with high quantum yield in the range 0.77-0.87 and 0.60-0.93, respectively. Park *et al.*⁷⁸ developed iridium(III) complexes with 2',6'-difluoro-4-methyl-2,3'-bipyridine as a cyclometalated ligand and introduced a variety of the ancillary ligands such as acetylacetonate, 2-picolinate or 2-(5-methyl-2H-1,2,4-triazol-3-yl)pyridinate to the iridium center to compare the effect of the ancillary ligands on the emission properties. These complexes exhibited blue emission at 447, 440 and 425 nm in CH₂Cl₂ solutions. However, the emission intensities of these complexes have not been quantified. More recently, Kessler and coworkers⁷⁹ have developed a novel bis-heteroleptic iridium(III) complex based on 4-(*tert*-butyl)-2',6'-difluoro-2,3'-bipyridine and acetylacetonate as an ancillary ligand and investigated the photophysical as well as electroluminescent properties. The developed blue PhOLED showed superior performance compared to published results on similar complexes with a maximum power efficiency of over 30 lm W⁻¹, indicating the great interest in this class of compounds throughout the scientific community. A preliminary report on the electroluminescence of tris-(2',6'-difluoro-4-NMe₂-2,3'-bipyridinato-N,C4')iridium(III) and (2',6'-difluoro-4-O-alkyl-2,3'-bipyridinato-N,C4')iridium(III) picolinate has been disclosed by Lee and coworkers.^{80, 81}

It is clear from the literature review that no systematic correlations are reported on the photophysical properties of iridium(III) complexes involving 2',6'-difluoro-2,3'-bipyridine ligand with electron-withdrawing and electron-donating group substitutions on 4' position of the pyridyl moiety. This has

inspired us to design and develop a series of cyclometalated ligands by substituting electron-withdrawing (-CHO, -CF₃ and -CN) and electron-donating groups (-OMe and -NMe₂) at the 4' position on the pyridyl moiety of the cyclometalated ligand, 2',6'-difluoro-2,3'-bipyridine and utilized for the construction of a series of iridium(III) compounds in the presence of picolinate as an ancillary ligand (Chart 1). The designed new iridium(III) compounds have been well characterized by various spectroscopic techniques and their electrochemical and photophysical properties have been investigated. Density functional theory calculations are used to rationalize the differences in the photophysical behaviour observed upon changes of the ligands. Finally, the developed compounds have been successfully used as dopants in 4,4'-bis(*N*-carbazolyl)-1,1'-biphenyl (CBP) as a host material and multilayer PhOLED devices have been fabricated and investigated electroluminescence properties.

Chart 1



Experimental Section

General information and materials.

A Bruker 500 MHz NMR spectrometer was used to record the ¹H, ¹⁹F and ¹³C NMR spectra of the complexes in CDCl₃ solution. The chemical shifts (δ) of the signals are given in ppm and referenced to the internal standard tetramethylsilane (TMS). The signals splitting are abbreviated as follows: *s* = singlet; *d* = doublet; *t* = triplet; *q* = quartet; *m* = multiplet. All coupling constants (*J*) are given in Hertz (Hz). Electrospray ionization (ESI) mass spectrum was recorded on a Thermo Scientific Exactive Benchtop LC/MS Orbitrap Mass Spectrometer. Matrix assisted laser desorption ionization time-of-flight (MALDI-TOF) mass spectrum was recorded on KRATOS analytical spectrometer (Shimadzu Inc.). Elemental analyses for C, H, and N were performed on an Elementar - vario MICRO cube elemental analyzer. The complex doped PMMA films were prepared by spin coating on to a 2 cm × 2 cm glass plate for 60s at a spin speed of 1000 rpm. Sodium hydride,

iodomethane, sodium carbonate, tetrakis(triphenyl phosphine) palladium(0), 2,6-difluoropyridine-3-boronic acid, 2-bromo-4-aminopyridine, 2-bromo-4-(trifluoromethyl) pyridine, 2-bromo-4-formylpyridine, 2-bromo-4-cyanopyridine, 2-bromo-4-methoxy pyridine, picolinic acid and $\text{IrCl}_3 \cdot x(\text{H}_2\text{O})$ were purchased from Alfa Aesar and were used without any further purification. The cyclometalated ligands, namely, 2',6'-difluoro-4-(formyl)-2,3'-bipyridine [CHODfppy] (**L1**), 2',6'-difluoro-4-(trifluoromethyl)-2,3'-bipyridine [CF₃dfppy] (**L2**) and 2',6'-difluoro-4-(cyano)-2,3'-bipyridine [CNdfppy] (**L3**) were first time synthesized and fully characterized. Other cyclometalating ligands such as 2',6'-difluoro-4-(methoxy)-2,3'-bipyridine [OMedfppy] (**L4**), 2',6'-difluoro-4-(N,N-dimethylamine)-2,3'-bipyridine [NMe₂dfppy] (**L5**), and precursor for **L5** namely, 2-bromo-4-N,N-dimethylaminopyridine (**L5a**) were synthesized according to previously reported procedures.^{80,81}

The iridium dimer complexes $[(\text{C}^{\text{A}}\text{N})_2\text{Ir}(\mu\text{-Cl})_2]$ ($\text{C}^{\text{A}}\text{N}$ = CHODfppy or CF₃dfppy or CNdfppy or OMedfppy or NMe₂dfppy) were synthesized using $\text{IrCl}_3 \cdot x(\text{H}_2\text{O})$ and CHODfppy or CF₃dfppy or CNdfppy or OMedfppy or NMe₂dfppy in a mixture of 2-ethoxyethanol and water according to literature method.⁸²⁻⁸⁴ Reactions were monitored by thin layer chromatography (TLC). Commercial TLC plates (silica gel 60 F254, Merck Co.) were used and the spots were observed under UV light at 254 and 365 nm. Silica column chromatography was performed using silica gel (230–400 mesh, Merck Co.) The dry solvents were used as received from Merck Millipore. All other reagents of analytical grade were used as received from Alfa Aesar, unless otherwise stated.

Synthesis of ligands and complexes.

Synthesis of 2-bromo-4-N,N-dimethylaminopyridine (L5a): To a suspension of sodium hydride (1.38 g, 34.6 mmol, 60% dispersion in mineral oil) in THF (20 mL) at 0°C, 2-bromo-4-aminopyridine (2.00 g, 11.56 mmol) was added. The reaction mixture was stirred for 30 min under argon atmosphere at the same temperature. After methyl iodide (4.10g, 28.90 mmol) was added, the resultant mixture was stirred at room temperature for 3 h. The reaction was quenched with water and organic materials were extracted with ethyl acetate. The combined extracts were washed with brine and dried over Na₂SO₄. After removal of solvents under reduced pressure, the residue was recrystallized from ethanol (1.30 g, 6.46 mmol, 55.8%). ¹H NMR (CDCl₃, 500 MHz): δ 7.94 (d, *J* = 5Hz, 1H), 6.64 (d, *J* = 2Hz, 1H), 6.44-6.43 (m, 1H), 2.99 (s, 6H). ¹³C NMR (CDCl₃, 126 MHz): δ 155.79, 149.30, 143.11, 109.27, 106.20, 39.24. MS (ESI): *m/z* 203.00 [*M*⁺].

General synthesis of cyclometalating ligands.

To a suspension of one equivalent of substituted bromopyridine [2-bromo-4-formylpyridine or 2-bromo-4-(trifluoromethyl) pyridine or 2-bromo-4-(cyano)pyridine or 2-bromo-4-methoxy pyridine or 2-bromo-4-(N,N-dimethylamino)pyridine] with 1.2 equivalents of 2,6-difluoropyridyl-3-boronic and 0.06 equivalents of tetrakis(triphenylphosphine)palladium(0) were dissolved in 25 ml of dry THF. A solution of 5% Na₂CO₃ (10 mL) was added and the mixture was refluxed with stirring for 24 h, under nitrogen

atmosphere. After being cooled, the mixture was poured into water, and extracted with ethyl acetate. The organic layer was dried over Na₂SO₄. The solvent was removed under reduced pressure to give a crude residue. The crude product was then purified by silica column chromatography with ethyl acetate: *n*-hexane (1: 9) as the eluent to give the final product.

2',6'-difluoro-4-(formyl)-2,3'-bipyridine [CHODfppy] (L1). Yield: 69%. ¹H NMR (CDCl₃, 500 MHz): δ 10.16 (s, 1H); 8.98 (d, *J* = 5Hz, 1H); 8.79-8.74 (m, 1H); 8.29 (s, 1H); 7.74 (t, *J* = 5Hz, 1H); 7.04-7.02 (m, 1H). ¹³C NMR (CDCl₃, 126 MHz): δ 191.07, 162.60, 160.60, 159.68, 152.19, 151.23, 146.14, 142.56, 122.84, 121.17, 107.37. ¹⁹F NMR (CDCl₃, 470 MHz): δ -68.51, -66.49. MS (ESI): *m/z* 221.05 [*M*⁺].

2',6'-difluoro-4-(trifluoromethyl)-2,3'-bipyridine [CF₃dfppy] (L2). Yield: 65%. ¹H NMR (CDCl₃, 500 MHz): δ 8.90 (d, *J* = 5Hz, 1H), 8.77-8.72 (m, 1H), 8.09 (s, 1H), 7.54 (d, *J* = 5Hz, 1H), 7.03-7.01 (m, 1H). ¹³C NMR (CDCl₃, 126 MHz): δ 162.59, 160.59, 157.52, 151.74, 150.79, 146.18, 123.73, 121.55, 119.29, 118.65, 107.37. ¹⁹F NMR (CDCl₃, 470 MHz): δ -68.56, -66.29, -64.93. MS (ESI): *m/z* 261.04 [*M*⁺].

2',6'-difluoro-4-(cyano)-2,3'-bipyridine [CNdfppy] (L3). Yield: 62%. ¹H NMR (CDCl₃, 500 MHz): δ 8.90 (t, *J* = 5Hz, 1H); 8.78-8.73 (m, 1H); 7.66 (s, 1H); 8.12 (s, 1H); 7.54-7.45 (m, 1H); 7.04-7.01 (m, 1H). ¹³C NMR (CDCl₃, 126 MHz): δ 162.81, 160.93, 157.68, 151.76, 150.80, 146.10, 125.30, 124.38, 121.61, 116.24, 107.60. ¹⁹F NMR (CDCl₃, 470 MHz): δ -68.10, -65.45. MS (ESI): *m/z* 218.05 [*M*⁺].

2',6'-difluoro-4-(methoxy)-2,3'-bipyridine [OMedfppy] (L4). Yield: 64%. ¹H NMR (CDCl₃, 500 MHz): δ 8.69-8.64 (m, 1H); 8.53 (d, 5.5Hz, 1H); 7.38 (s, 1H); 6.97-6.95 (m, 1H); 6.84-6.83 (m, 1H); 3.91 (s, 3H). ¹³C NMR (CDCl₃, 126 MHz): δ 162.11, 160.14, 157.29, 151.80, 150.90, 146.18, 119.05, 110.39, 109.08, 106.90, 55.29. ¹⁹F NMR (CDCl₃, 470 MHz): δ -69.22, -68.04. MS (ESI): *m/z* 223.06 [*M*⁺].

2',6'-difluoro-4-(N,N-dimethylamine)-2,3'-bipyridine [NMe₂dfppy] (L5). Yield: 60%. ¹H NMR (CDCl₃, 500 MHz): δ 8.63-8.58 (m, 1H), 8.31 (d, *J* = 6Hz, 1H), 7.03 (s, 1H), 6.94-6.92 (m, 1H), 6.52-6.50 (m, 1H), 3.07 (s, 6H). ¹³C NMR (CDCl₃, 126 MHz): δ 161.66, 159.81, 154.82, 150.55, 149.73, 146.25, 120.29, 106.95, 106.45, 105.97, 39.24. ¹⁹F NMR (CDCl₃, 470 MHz): δ -69.07, -69.60. MS (ESI): *m/z* 236.09 [*M*⁺].

Synthesis of iridium(III) dimer complex

Synthesis of $[(\text{CHODfppy})_2\text{Ir}(\mu\text{-Cl})_2]$. $\text{IrCl}_3 \cdot x\text{H}_2\text{O}$ (224.36 mg, 0.75 mmol) and CHODfppy (**L1**) (350 mg, 1.58 mmol) were dissolved in 20 mL of 2-ethoxyethanol and water (8:2) mixture and refluxed at 140°C for 24 h. After the solution was cooled, the addition of 40 mL of H₂O gave a pale yellow precipitate that was filtered and washed with diethyl ether. The crude product was used for the next reaction without further purification (yield: 55%).

Synthesis of $[(\text{CF}_3\text{dfppy})_2\text{Ir}(\mu\text{-Cl})_2]$. $\text{IrCl}_3 \cdot x\text{H}_2\text{O}$ (191.36 mg, 0.64 mmol) and CF₃dfppy (**L2**) (350 mg, 1.34 mmol) were dissolved in 20 mL of 2-ethoxyethanol and water (8:2) mixture and refluxed at 140 °C for 24 h. After the solution was cooled, the addition of 40 mL of H₂O gave a yellow precipitate that was filtered and washed with diethyl ether. The crude product

was used for the next reaction without further purification (yield: 60%).

Synthesis of [(CNdfppy)₂Ir(μ-Cl)]₂. IrCl₃·xH₂O (227.47 mg, 0.76 mmol) and CNdfppy (**L3**) (350 mg, 1.61 mmol) were dissolved in 20 mL 2-ethoxyethanol and water (8:2) mixture and refluxed at 140 °C for 24 h under dry and inert conditions. After the solution was cooled, the addition of 40 mL of H₂O gave an orange precipitate that was filtered and washed with diethyl ether. The crude product was used for the next reaction without further purification (yield: 40%).

Synthesis of [(OMedfppy)₂Ir(μ-Cl)]₂. IrCl₃·xH₂O (222.38 mg, 0.74 mmol) and OMedfppy (**L4**) (350 mg, 1.57 mmol) were dissolved in 20 mL 2-ethoxyethanol and water (8:2) mixture and refluxed at 140 °C for 24 h. After the solution was cooled, the addition of 40 mL of H₂O gave a pale yellow precipitate that was filtered and washed with diethyl ether. The crude product was used for the next reaction without further purification (yield: 67%).

Synthesis of [(NMe₂dfppy)₂Ir(μ-Cl)]₂. IrCl₃·xH₂O (211.36 mg, 0.70 mmol) and NMe₂dfppy (**L5**) (350 mg, 1.48 mmol) were dissolved in 20 mL 2-ethoxyethanol and water (8:2) mixture and refluxed at 140 °C for 24 h. After the solution was cooled, the addition of 40 mL of H₂O gave a pale yellow precipitate that was filtered and washed with diethyl ether. The crude product was used for the next reaction without further purification (yield: 60%).

General synthesis procedure for complexes Ir1–Ir5.

A mixture of one equivalent of the corresponding dimer, 2.6 equivalents of picolinic acid and 11 equivalents of sodium carbonate were stirred overnight in a mixture (3:1) of dichloromethane and ethanol (40 mL) at 60 °C under argon atmosphere. The solvent was removed by evaporation under reduced pressure. The crude product obtained was poured into water and extracted with ethyl acetate (3 × 50 mL). The combined organic layer was dried over Na₂SO₄. The solvent was removed under reduced pressure to give a crude residue. The crude product was purified by using silica gel column chromatography with CH₂Cl₂: methanol in 9:1 ratio as eluent, giving the desired complex as light yellow powder with the following yields: **Ir1** (65%), **Ir2** (80%), **Ir3** (36%), **Ir4** (90%) and **Ir5** (76%). All purified samples were recrystallized and vacuum dried before conducting all analysis

Spectral data of (CHOdppy)₂Ir(pic), Iridium(III) (2',6'-difluoro-4-(formyl)-2,3'-bipyridinato-N,C4') (picolinate) (Ir1). ¹H NMR (CDCl₃, 500 MHz): δ 10.23 (s, 2H); 9.08 (d, *J* = 6Hz, 1H); 8.73-8.68 (m, 2H); 8.42-8.41 (m, 1H); 8.12-8.07 (m, 1H); 7.79-7.68 (m, 3H); 7.60-7.52 (m, 2H); 5.84 (s, 1H); 5.55 (s, 1H). ¹⁹F NMR (CDCl₃, 470 MHz): δ -67.63, -67.01, -66.66, -65.96. MALDI-TOF calcd for C₂₈H₁₄F₄IrN₅O₄ 754.49 ([M+H]⁺); found 755.49. Elem. anal. Calcd (%) for C₂₈H₁₄F₄IrN₅O₄: C, 44.68; H, 1.89; N, 9.30. Found: C, 44.36; H, 2.10; N, 9.21.

Spectral data of (CF₃dfppy)₂Ir(pic), Iridium(III) (2',6'-difluoro-4-(trifluoromethyl)-2,3'-bipyridinato-N,C4') (picolinate) (Ir2). ¹H NMR (CDCl₃, 500 MHz): δ 9.00 (d, *J* = 6Hz, 1H), 8.47 (s, 1H), 8.53 (s, 1H), 5.54 (s, 1H), 8.41 (d, *J* = 7.5Hz, 1H), 8.12 (t, *J* = 15.5Hz, 1H), 7.77 (d, *J* = 5Hz, 1H), 7.58 (s, 1H), 7.55 (d, *J* = 5.5Hz, 1H), 7.34 (d, *J* = 6Hz, 1H), 5.86 (s, 1H). ¹⁹F NMR (CDCl₃,

470 MHz): δ -67.22, -66.57, -66.27, -65.66, -65.04, -64.84. MALDI-TOF calcd for C₂₈H₁₂F₁₀IrN₅O₂ 833.05 ([M+H]⁺); found 832.99. Elem. anal. Calcd (%) for C₂₈H₁₂F₁₀IrN₅O₂: C, 40.39; H, 1.45; N, 8.41. Found: C, 40.51; H, 1.61; N, 8.21.

Spectral data of (CNdfppy)₂Ir(pic), Iridium(III) (2',6'-difluoro-4-(cyano)-2,3'-bipyridinato-N,C4') (picolinate) (Ir3). ¹H NMR (CDCl₃, 500 MHz): δ 9.01(d, 1H, *J* = 6Hz); 8.57 (s, 1H); 8.51 (s, 1H); 8.43 (d, *J* = 7.5Hz, 1H); 8.15-8.11 (m, 1H); 7.75 (d, 1H, *J* = 5Hz); 7.63-7.60 (m, 2H); 7.56-7.54 (m, 1H); 7.33-7.32 (m, 1H); 5.84 (s, 1H); 5.54 (s, 1H). ¹⁹F NMR (CDCl₃, 470 MHz): δ -66.13, -65.51, -65.39, -64.80. MALDI-TOF calcd for C₂₈H₁₂F₄IrN₅O₂ 747.70 ([M+H]⁺); found 748.90. Elem. anal. Calcd (%) for C₂₈H₁₂F₄IrN₅O₂: C, 45.04; H, 1.62; N, 13.13. Found: C, 44.84; H, 1.79; N, 12.93.

Spectral data of (OMedfppy)₂Ir(pic), Iridium(III) (2',6'-difluoro-4-methoxy-2,3'-bipyridinato-N,C4')(picolinate) (Ir4). ¹H NMR (CDCl₃, 500 MHz): δ 8.52 (d, 1H, *J* = 5Hz); 8.37 (d, 8Hz, 1H); 8.03-8.00 (m, 1H); 7.81-7.75 (m, 3H); 7.51- 7.48 (m, 1H); 7.20 (d, 1H, *J* = 6.5Hz); 6.86-6.84 (m, 1H); 6.66-6.64 (m, 1H); 4.02 (d, *J* = 3Hz, 6H); 5.89 (s, 1H); 5.64 (s, 1H). ¹⁹F NMR (CDCl₃, 470 MHz): δ -70.85, -70.21, -69.40, -68.78. MALDI-TOF calcd for C₂₈H₁₈F₄IrN₅O₄ 757.94 ([M+H]⁺); found 758.94. Elem. anal. Calcd (%) for C₂₈H₁₈F₄IrN₅O₄: C, 44.44; H, 2.40; N, 9.26. Found: C, 44.62; H, 2.48; N, 9.08.

Spectral data of (NMe₂dfppy)₂Ir(pic), Iridium(III) (2',6'-difluoro-4-(N,N-dimethylamine)-2,3'-bipyridinato-N,C4') (picolinate) (Ir5). ¹H NMR (CDCl₃, 500 MHz): δ 8.33 (d, *J* = 3Hz, 1H), 8.19 (d, *J* = 7Hz, 1H), 7.97-7.94 (m, 1H), 7.78 (d, *J* = 5Hz, 1H), 7.45-7.39 (m, 3H) 6.93 (d, *J* = 7Hz, 1H), 6.46-6.44 (m, 1H), 6.26-6.24 (m, 1H), 5.95 (s, 1H), 5.74 (s, 1H) 3.18 (d, *J* = 5Hz, 12H). ¹⁹F NMR (CDCl₃, 470 MHz): δ -73.15, -72.48, -71.08, -70.57. MALDI-TOF calcd for C₃₀H₂₄F₄IrN₇O₂ 785.16 ([M+H]⁺); found 785.52. Elem. anal. Calcd (%) for C₃₀H₂₄F₄IrN₇O₂: C, 46.03; H, 3.09; N, 12.53. Found: C, 45.81; H, 3.26; N, 12.44.

X-ray crystallographic analysis.

The diffraction data of single crystal was collected on a Rigaku Saturn 724+ diffractometer using graphite monochromated Mo-Kα radiation. The data was processed with the Rigaku Crystal Clear software.^{85, 86} The structure solution was carried out by direct methods, and the refinements were performed by full-matrix least-squares on *F*² using the SHELXTL suite of programs.⁸⁷ All of the hydrogen atoms were placed in geometrically ideal positions (using corresponding HFIX) and refined in the riding mode. Final refinement included the atomic positions of all the atoms, anisotropic thermal parameters for all of the non-hydrogen atoms, and isotropic thermal parameters for all of the hydrogen atoms. The disordered solvent molecules could not be adequately modeled. The bypass procedure in Platon (Spek, 1990) was used to remove the electronic contribution from these solvents. For complex **Ir2**, the total potential solvent (dichloromethane and water) accessible void volume was 2519 Å³ (which is 34% of the unit cell volume) and the electron count/cell = 606.

Thermal analysis.

Thermo-gravimetric analyses were performed on an EXSTAR TG-DTA 6200 instrument (SII Nanotechnology Inc.) heated

from 30 to 1000 °C in flowing of nitrogen at the heating rate of 10 °C min⁻¹. Temperature at which a 5% weight loss occurred has been considered as the decomposition temperature (T_d). Differential scanning calorimetry was performed using a TA Q20 general-purpose DSC instrument in sealed aluminum pans under nitrogen flow at a heat/cooling rate of 5 °C/min. The endothermic peak observed in the second heating cycle has been considered as the glass transition temperature (T_g).

Photophysical characterization.

The electronic absorption spectrum of the complex was measured on a Shimadzu, UV-2450 UV-vis-NIR spectrophotometer. The photoluminescence (PL) spectrum of the iridium(III) complex was recorded on a Spex-Fluorolog FL22 spectrofluorimeter equipped with a double grating 0.22 m Spex 1680 monochromator and a 450 W Xe lamp as the excitation source and a Hamamatsu R928P photomultiplier tube detector. Emission and excitation spectra were corrected for source intensity (lamp and grating) by standard correction curves. Phosphorescence lifetimes were measured using IBH (Fluoro Cube) time-correlated pico second single photon counting (TCSPC) system. A pulsed diode laser (<100 ps pulse duration) at a wavelength of 375 nm (Nano LED-10) were used to excite at the MLCT states of the complexes with a repetition rate of 50 KHz. The detection system consists of a microchannel plate photomultiplier (5000 U-09B, Hamamatsu) with a 38.6 ps response time coupled to a monochromator (5000M) and TCSPC electronics (Data Station Hub including Hub-NL, Nano LED controller and preinstalled Fluorescence Measurement and Analysis Studio (FMAS) software). The phosphorescence lifetime values were determined by deconvoluting the instrument response function with mono-exponential decay using DAS6 decay analysis software. The quality of the fit has been judged by the fitting parameters such as χ^2 (<1.2) as well as the visual inspection of the residuals. The luminescence quantum efficiencies in the solution state were calculated by a comparison of the emission intensities (integrated areas) of a standard sample and the unknown sample according to eq 1.

$$\Phi_{\text{unk}} = \Phi_{\text{std}}(I_{\text{unk}}/I_{\text{std}})(A_{\text{std}}/A_{\text{unk}})(\eta_{\text{unk}}/\eta_{\text{std}})^2 \quad (1)$$

where Φ_{unk} and Φ_{std} are the luminescence quantum yields of the unknown sample and standard sample, respectively. I_{unk} and I_{std} are the integrated emission intensities of the unknown sample and standard sample solution, respectively. A_{unk} and A_{std} are the absorbances of the unknown sample and standard sample solution at their excitation wavelengths, respectively. The η_{unk} and η_{std} terms represent the refractive indices of the corresponding solvents (pure solvents were assumed). Quinine sulphate monohydrate ($\Phi_p = 0.54$) in 0.05 M H₂SO₄ has been used as a standard for the blue emitting complex Ir4.⁸⁸ Ir(ppy)₃ has been used as a standard for green emitting complexes Ir1-Ir3 and Ir5.⁸⁹ All solutions for the photophysical studies were deaerated with pre-purified Argon gas prior to the measurements. Solid state photoluminescence quantum yield of the PMMA films measured by absolute method using a calibrated integrating sphere in a SPEX Fluorolog Spectrofluorimeter on the basis of the de Mello method.⁹⁰

Cyclic voltammetry.

Cyclic voltammetry experiments were carried out with a BAS 50W voltammetric analyzer using three electrode cell assemblies. Platinum wires were used for counter electrodes, a silver wire was used as Ag/Ag⁺ quasi reference electrode and a platinum electrode was used as a working electrode. Measurements were carried out in acetonitrile solution with tetrabutylammonium hexafluorophosphate as supporting electrolyte at a scan rate of 100 mV/s. Concentrations of iridium(III) complex and supporting electrolyte were 5 × 10⁻³ and 0.1M, respectively. The ferrocenium/ferrocene couple (FeCp₂⁺/FeCp₂⁰) was used as an internal reference. The energy level of FeCp₂⁺/FeCp₂⁰ was assumed at -4.8 eV to vacuum.⁹¹ All solutions for the electrochemical studies were deaerated with pre-purified argon gas prior to the measurements.

Computational methods.

The geometrical structures of the singlet ground state (S0) and the lowest lying triplet excited state (T1) were optimized by using density functional theory (DFT) based on a method with Becke's three-parameter functional and the Lee-Yang-Parr functional (B3LYP)^{92,93} with LANL2DZ basis set for the Iridium (Ir) atom and 6-31G* for the rest of the atoms. Frequency calculations were also executed at the same level of theory. The optimizations and the vibrational data confirmed that the structures were true minima on the potential energy surface because there were no imaginary frequencies. On the basis of the optimized ground and excited state geometry structures, the absorption spectral properties in dichloromethane media were calculated by time-dependent density functional theory (TD-DFT) approach with (B3LYP/6-31G*). As solvent effects are known to play a crucial role in predicting the absorption and emission spectra, the same was incorporated in the TD-DFT calculations within the PCM framework. The Swizard program has been employed to evaluate the contribution of singly excited state configurations to each electronic transition.⁹⁴ All calculations were carried out with Gaussian 09 package.⁹⁵

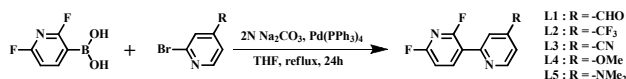
PhOLED device fabrication

PhOLEDs were fabricated on indium-tin oxide (ITO) coated glass substrates (sheet resistance of 20 ohm/sq) by first cleaning them using trichloroethylene, acetone, and isopropyl alcohol and deionized water sequentially for 20 min using an ultrasonic bath and dried in flowing nitrogen. Prior to film deposition, the ITO substrates were treated with UV-ozone for 5 min. Organic materials and cathode were sequentially deposited under a high vacuum (4 × 10⁻⁷ torr). The deposition rate of organic materials was kept at 6 nm/min, whereas the deposition rates of LiF and Al were 0.6 nm/min and 30 nm/min, respectively. Thickness of the deposited layers was monitored by an in-situ quartz crystal monitor. The cathode was deposited on the top of the structure through a shadow mask. Used device structure was ITO (120 nm)/F₄-TCNQ (2.5 nm)/α-NPD (45 nm)/Emissive layer (30 nm)/BCP (6 nm)/Alq₃ (30 nm)/LiF (1 nm)/Al (150 nm). N,N-Diphenyl-N',N'-bis(1-naphthyl)-1,1'-biphenyl-4,4'-diamine (α-NPD (Sigma Aldrich) was used as a hole transport layer, 4,4'-Bis(N-carbazolyl)-1,1'-biphenyl (CBP) as host layer with 5 wt% doped iridium complex Ir2-Ir4 was used as emissive layer, 2,9-dimethyl-4,7-diphenyl-

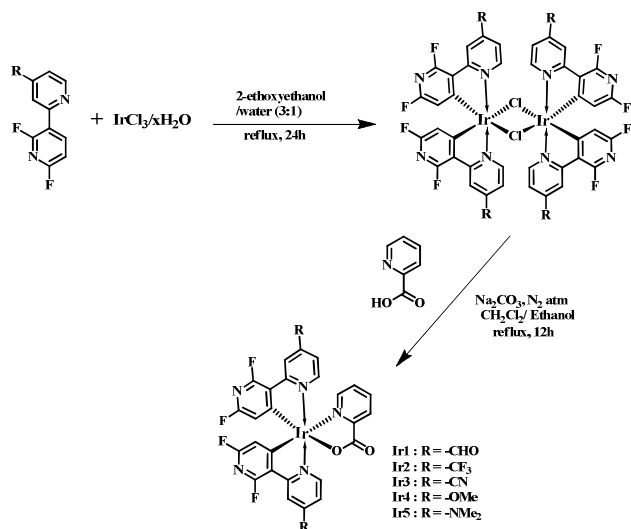
1,10-phenanthroline (BCP) as hole blocking layer, tris(8-hydroxyquinoline)-aluminium (Alq₃, Sigma Aldrich) as electron transport layer, LiF (Merck, Germany) as electron injection layer and Al as the cathode. 2,3,5,6-tetrafluoro-7,7',8,8'-tetracyanoquinodimethane (F₄-TCNQ) is utilized for efficient hole injection from ITO to α -NPD and its thickness is used as optimized by P. Tyagi et al.⁹⁶ for enhanced efficiency and life time of PhOLEDs. Synthesized materials **Ir2**, **Ir3** and **Ir4** were mixed in CBP with 5 wt % concentration for using them as the emissive layer. The size of each pixel was 3x4 mm². The EL spectra were measured using an Ocean Optics high resolution spectrometer (HR-2000CG UV-NIR). The J-V-L characteristics were measured with a luminance meter (LMT I-1009) and a Keithley 2400 programmable voltage-current digital source meter. All the measurements were carried out at room temperature under ambient conditions.

Results and Discussion

Synthesis and characterization.



Scheme 1 Synthetic routes of cyclometalating ligands L1-L5



Scheme 2 Synthetic routes of heteroleptic Ir³⁺ complexes Ir1-Ir5

The C^N chelating ligands used in the current study were synthesized by conventional Suzuki coupling reaction of corresponding 2-bromopyridine with 2,6-difluoropyridinyl-3-boronic acid in the presence of sodium carbonate and tetrakis(triphenylphosphine) palladium(0) as a catalyst as shown in scheme 1. It is important to mention that pure ligands could only be obtained after column chromatographic separations. The dimer precursors to obtain iridium(III) complexes **Ir1-Ir5** were prepared by a standard procedure proposed by Watts and co-workers.⁸³ The μ -chloro bridged

dimer was formed through the reaction of cyclometalated ligand precursor with IrCl₃.H₂O in a mixture of 2-ethoxyethanol and water. The new iridium complexes **Ir1-Ir5** were obtained in the presence of Na₂CO₃ via the reaction of μ -chloro bridged dimer and the ancillary ligand picolinic acid.^{79,97} A pictorial synthetic pathways leading to the designed iridium(III) compounds is depicted in scheme 2. After purification and recrystallization of the compounds detailed characterizations were carried out by ¹H, ¹⁹F and ¹³C NMR, MALDI-TOF Mass spectrometry (Figs. S1 – S38 ESI[†]) and elemental analyses.

X-ray single crystal structures.

Single crystals of **Ir2** and **Ir4** have been grown by slow diffusion of hexane into a dichloromethane solution of the complexes. The compounds **Ir2** and **Ir4** were structurally authenticated by

Table 1 Crystallographic and refinement data for complexes **Ir2** and **Ir4**

	Ir2	Ir4
Formula	C ₂₈ H ₁₈ F ₄ Ir N ₅ O ₂	C ₂₈ H ₁₈ F ₄ Ir N ₅ O ₄
Formula weight	724.67	841.60
Temp (K)	301(2)	150(2)
Wavelength (Å)	0.71073	0.71073
Crystal system	Orthorhombic	monoclinic
Space group	<i>Pbca</i>	<i>P2₁/c</i>
Crystal size (mm ³)	0.20 × 0.20 × 0.20	0.50 × 0.40 × 0.30
<i>a</i> [Å]	16.765(2)	12.069(3)
<i>b</i> [Å]	15.096(8)	12.029(3)
<i>c</i> [Å]	20.6420(10)	19.562(5)
α [°]	90.00	90.00
β [°]	90.00	92.19
γ [°]	90.00	90.00
<i>V</i> [Å ³]	5224(3)	2837.8(11)
<i>Z</i>	8	4
ρ_{calc} [g/cm ³]	1.843	1.970
μ (Mo K α) [mm ⁻¹]	5.176	4.967
Total reflections	31043	24916
Unique reflections	5260	6465
$R_f, R_w(F^2)$ [$I > 2\sigma(I)$]	0.0772, 0.1937	0.0250, .0530
GOF on F^2	1.048	1.047
CCDC	973778	1005716

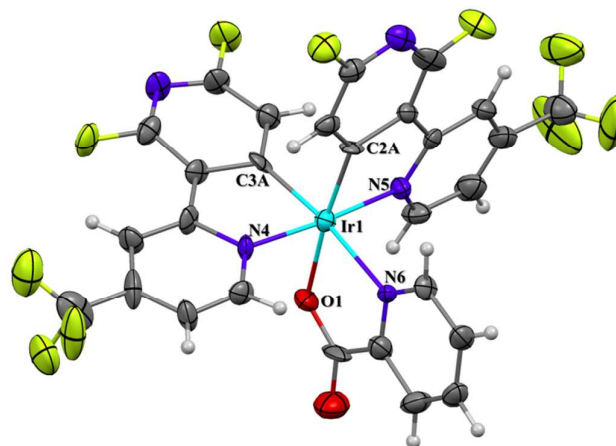


Fig. 1 Crystal structure of complex **Ir2** with atom numbering scheme. Selected bond lengths (Å) and angles (°): Ir(1)–C(3A) 1.966(16), Ir(1)–C(2A) 1.987(10), Ir(1)–O(1) 2.115(11), Ir(1)–N(6) 2.150(11), Ir(1)–N(5) 2.045(11), Ir(1)–N(4) 2.026(10); N(4)–Ir(1)–N(6) 175.2(5), C(3A)–Ir(1)–N(6) 172.5(5), C(2A)–Ir(1)–O(1) 174.5(5).

X-ray single-crystal diffraction and the corresponding molecular structures are depicted in Figs. 1 and 2, respectively. Selected crystallographic data and structure refinement parameters are given in Table 1. Both the iridium(III) complexes adopt a distorted octahedral geometry around the Ir³⁺ centre with N-binding pyridines in trans positions in relative to each other. These results are in good agreement with that of earlier disclosed X-ray single crystal structure of (dfppy)₂Irpic.¹⁵ Overall the geometry around the metal is not significantly influenced by the various substituted cyclometalated ligands. The bond lengths of Ir–C, Ir–N and Ir–O for **Ir2** and **Ir4** are within the range reported for those of related compounds (dfppy)₂Irpic¹⁵ and Irpic (Table 2 and

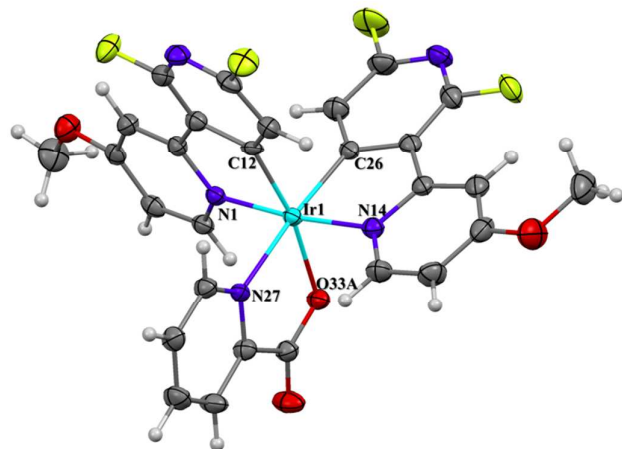


Fig. 2 Crystal structure of complex **Ir4** with atom numbering scheme. Selected bond lengths (Å) and angles (°): Ir(1)–C(12) 1.983(2), Ir(1)–C(26) 2.000(3), Ir(1)–O(33A) 2.158(2), Ir(1)–N(1) 2.048(2), Ir(1)–N(14) 2.050(2), Ir(1)–N(27) 2.154(5); N(1)–Ir(1)–N(14) 173.7(9), C(26)–Ir(1)–N(27) 174.7(9), C(12)–Ir(1)–O(33A) 169.2(9).

Table 2 Average of selected bond lengths (Å) and angles (°) for complexes **Ir2**, **Ir4** and **Ir(dfppy)₂pic^a**

Bond length	Ir2	Ir4	Ir(dfppy)₂pic^a
Ir–N	2.035(11)	2.049(2)	2.049(7)
Ir–C	1.991(10)	1.991(2)	2.001(7)
Ir–O	2.115(11)	2.158(2)	2.131(4)
Ir–N ₁	2.150(11)	2.125(2)	2.115(7)
C ₁ –C ₂	1.443(2)	1.461(3)	1.470(1)
Bond angles			
N–Ir–N	172.5	173.8	175.6
C–Ir–N ₁	172.5	174.8	168.8
C–Ir–O	174.5	169.2	174.5
C–Ir–C	87.42	88.20	90.61
O–Ir–N ₁	77.09	77.24	77.24
C–Ir–N	80.47	80.57	80.67
Torsion angle			
C ₂ –C ₃ –C ₄ –R	176.56	178.05	---

^a The average bond length and bond angle values for Ir(dfppy)₂pic were taken from ref 7.

Fig. S39 ESI†).^{75,98} However, there is a significant effect on C₁–C₂ bond lengths in cyclometalating ligand in the presence of electron-withdrawing and electron-donating substituents at

the C₄ position on the N-coordinating pyridine ring. Firstly, in the substitution of –CF₃ in the C₄ position shortens C₁–C₂ bond (1.443(2) Å) in **Ir2** that links both rings of the cyclometalating ligand as compared to unsubstituted parent compound (dfppy)₂Irpic (1.470(1) Å), due to the strong electron-withdrawing effect (Hammett constant: C_{σm} = 0.43) at the meta-C₂ position. However, in **Ir4**, the –OMe substitution moderately decreases the C₁–C₂ bond (1.461(3) Å). This can be explained on the basis of –OMe having positive C_{σm} value (0.12). Secondly, C₄' substituents (–CF₃ and –OMe in complexes **Ir2** and **Ir4**, respectively) on the N-coordinating pyridine ring tend to deviate slightly from the plane of the cyclometalating ring, as exemplified by the C₂–C₃–C₄–R torsion angles, due to the bulky nature of the substituents. The C(3A)–Ir(1)–N(6) bond angle [172.5(5)°] in **Ir2** and C(26)–Ir(1)–N(27) bond angle [174.78(9)°] in **Ir4** are found to be moderately distorted from linearity, which may be caused by intermolecular interactions. Several strong intermolecular interactions such as edge-to-face C–H...π(py), and hydrogen bonding via C(π)–H...F or C(π)–H...O or C(π)–H...N are in fact observed in the crystal lattices of **Ir2** and **Ir4**. The structural parameters and details for the intermolecular interactions can be found in the ESI (Tables S1 – S5 †).

Thermal properties.

The thermal properties of the **Ir1**–**Ir5** were investigated by thermogravimetric analysis (TGA) and differential scanning calorimetry (DSC) at a scanning rate of 5°C/min under a nitrogen atmosphere. As shown in Fig. S40 ESI†, **Ir3** and **Ir5** complexes are thermally stable with decomposition temperatures (T_d: at a 5% weight loss) higher than 415°C. On the other hand, the thermal stability of the –CHO, –CF₃ and –OMe substituted iridium(III) complexes **Ir1**, **Ir2** and **Ir4** are found to be in the range 362 – 367 °C (Table 3). Further, these compounds show glass transition temperatures (T_g: from the second heating cycle of the DSC curve) in the range 159–231°C, which guaranteed the morphological stability of the complexes (Fig. S41 ESI†).

Theoretical calculations.

The optimized geometries of the iridium(III) complexes obtained by DFT method are displayed in Fig. S42 ESI†. The modeled structures possess a distorted octahedral geometry around the iridium center, with C₁ point group symmetry. The Ir–C (mean value: 2.005 Å) and Ir–N (mean value: 2.068 Å) bond lengths in –OMe substituted iridium(III) complex (**Ir2**) obtained by structural optimization are in good agreement with the single crystal X-ray diffraction data [Ir–C (mean value: 2.035 Å) [Table S6 ESI†].

MO analysis indicated that the HOMO of electron-withdrawing group substituted iridium(III) complexes (**Ir1**–**Ir3**) is mainly localized on the 5d-orbitals of iridium metal (51–52%), π-orbitals of difluoropyridyl moiety of the cyclometalated bipyridine ligand (28–29%) and a small contribution from the picolinate ancillary ligand (11–13%) (Figs. 3–4 and Table S7 ESI†). The present observation is similar to that of the HOMO orbital distribution of (dfppy)Irpic reported elsewhere.⁷⁶ The LUMO is essentially localized on the substituted N-coordinated pyridyl moiety of the cyclometalated ligand (75–89%).

However, in the case of iridium(III) complex **Ir2**, the LUMO is not localized on the $-\text{CF}_3$ substituent. These results strongly indicate a HOMO-LUMO transition with MLCT character in these complexes (**Ir1–Ir3**) (Table S8 ESI†).

In the case of electron-donating group containing iridium(III) complexes, HOMO is localized on the 5d-orbitals of iridium atom (45–52%), π -orbitals of the substituted difluoropyridine ligand (35–40%) and picolinate ancillary ligand (12–14%). However, in the case of **Ir5** the HOMO contains major contribution from N-coordinated pyridyl moiety of the cyclometalated ligand (30%). On the other hand, LUMO is mainly localized on picolinate ancillary ligand (90–93%) with

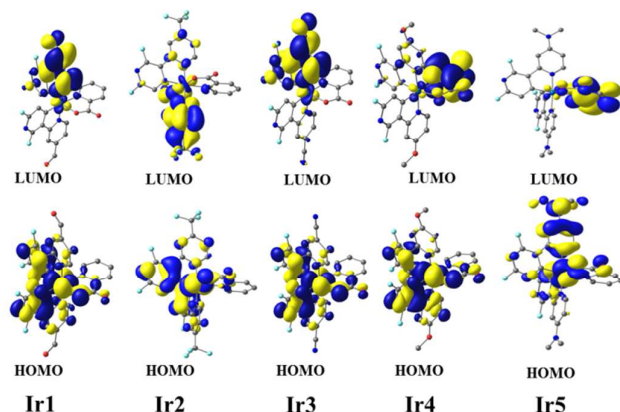


Fig. 3 Selected molecular orbital diagram indicating isodensity HOMO and LUMO surfaces for complexes **Ir1–Ir5**. All of the molecular orbital surfaces correspond to an isocontour value of $|\psi| = 0.03$.

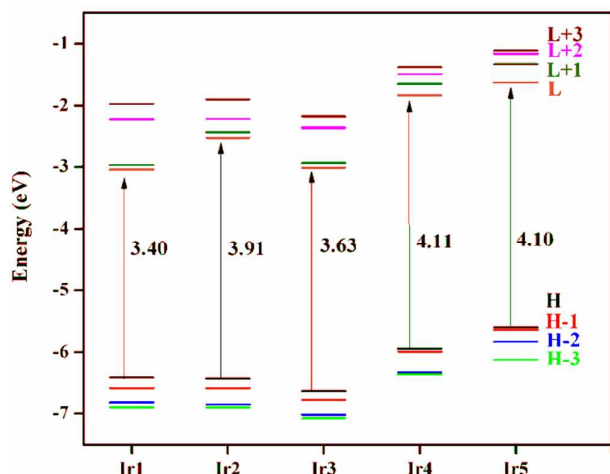


Fig. 4 Partial molecular orbital diagram for complexes **Ir1–Ir5**. The arrows are intended to highlight the calculated HOMO–LUMO energy gaps (H = HOMO, L = LUMO).

minor contribution from iridium metal center (2–3%) and cyclometalated ligand (4.3–7.1%). Thus the phosphorescence of electron-donating group substituted iridium(III) complexes may be described as mixed ^3LC and $^3\text{MLCT}$ transitions. These results are similar to that of unsubstituted $(\text{dfppy})_2\text{Ir}(\text{pic})$.⁷⁶

Electrochemical properties.

To understand the electronic effects caused by the substituent on the C4' position on the pyridyl moiety of the cyclometalated

ligand, cyclic voltammetry experiments of the complexes **Ir1–Ir5** were carried out using ferrocene as the internal standard (Figs. S43–S44 ESI†). The Highest Occupied Molecular Orbital (HOMO)/ Lowest Unoccupied Molecular Orbital (LUMO) for complexes **Ir1–Ir5** are listed in Table 3. The $E_{\text{onset}}(\text{oxd})$ value of the respective iridium(III) complex was determined using CV relative to a ferrocene/ferrocenium redox potential. All the iridium(III) complexes showed irreversible oxidation voltammograms. Kang and co-workers⁷⁶ also reported difficulties in observing reversible oxidation potential for the parent compound $(\text{dfppy})_2\text{Irpic}$. The investigations on DFT calculations indicate that the HOMO of electron-withdrawing

Table 3 Electrochemical and thermal properties of Ir^{3+} complexes **Ir1 – Ir5**

Complex	E_{ox}^a (V)	E_{red}^a (V)	HOMO ^b (eV)	LUMO ^c (eV)	$E_{\text{g(elec)}}^d$ (eV)	T_{g}^e (°C)	T_{d}^f (°C)
Ir1	1.75	-0.94	-6.07	-3.42	2.65	231	367
Ir2	1.70	-1.43	-6.06	-2.9	3.13	212	362
Ir3	1.78	-1.16	-6.13	-3.21	2.92	–	415
Ir4	1.57	-1.77	-5.93	-2.58	3.35	159	365
Ir5	1.21	-1.82	-5.57	-2.54	3.03	–	397

^aElectrochemical data versus $(\text{FeCp}_2^+/\text{FeCp}_2^0)$ (FeCp_2 is ferrocene) were collected in $\text{CH}_3\text{CN}/0.1$ M TBAH (tetra-butylammoniumhexafluorophosphate). ^bHOMO = $-[4.8 - (0.44) + E_{\text{oxd}}]$. ^cLUMO = $-[4.8 - (0.44) + E_{\text{red}}]$. ^dElectrochemical band gap. ^e T_{g} = glass transition temperature from DSC curve, T_{g} peak for **Ir3** and **Ir5** were not observed up to a temperature scan of 300°C. ^f T_{d} = decomposition temperature 5% weight loss from TG curve

Table 4 Swain–Lupton constants for the substituents⁹⁹

Substituent	F value	R value
-H	0.03	0.00
-CHO	0.33	0.09
-CF ₃	0.38	0.16
-CN	0.51	0.15
-OMe	0.29	-0.56
-NMe ₂	0.15	-0.98

group substituted iridium(III) complexes is localized at the iridium metal centre and the difluoropyridyl moiety. Thus the oxidation potentials are marginally influenced by the substitution of electron-withdrawing groups on pyridyl moiety of the cyclometalated ligand. On the other hand, the substitution of electron-donating group induces destabilization of HOMO and hence more negative shift of the oxidation peak potentials are noted (1.57 and 1.21 V for **Ir4** and **Ir5**). This can be due to more electron-donating features of the substituent groups in the pyridyl ring, which enhances the electron density at metal center through *ortho*-metalating nitrogen atom. Thus it becomes easier to remove the electrons from the HOMO. The $-\text{NMe}_2$ substituted **Ir5** shows the lowest oxidation potential among the series (1.21 V). As per the DFT calculations, the HOMO of **Ir5** is mainly localized on iridium metal center, N-coordinated pyridine ring and the electron-donating $-\text{NMe}_2$ substituent. Hence the first quasi reversible oxidation potential observed at 1.21 V in complex **Ir5** may be due to the oxidation of $-\text{NMe}_2$ substituent in the pyridine ring. All the iridium(III) complexes except **Ir1** and **Ir2** display reversible reduction potentials. The first reduction peak potential is observed at -0.94, -1.43, -1.16, -1.77 and -1.82 V,

respectively, for **Ir1-Ir5**. The second reduction potential is detected at -1.66 and -1.31 V for **Ir1** and **Ir3**, respectively. However, the second reduction peak in the case of **Ir2**, **Ir4** and **Ir5** could not be obtained in the limit of the potential window of the experimental conditions. Since the LUMO orbitals are localized on the picolinate ancillary ligand in **Ir4** and **Ir5**, the substitution of electron-donating groups on the pyridyl moiety of the cyclometalated ligand shows a marginal effect on the reduction potentials of these complexes. However, the substitution of electron-withdrawing groups such as $-\text{CF}_3$ and $-\text{CN}$ in **Ir2** and **Ir3** induces the stabilization of LUMO, which could be observed as a more positive shift of the reduction peak potential. The Swain-Lupton constant as a modification of the Hammett rule can be used as electron accepting and donating parameter in explaining the observed reduction

behaviour of these complexes. As shown in Table 4, a larger F value is more σ -electron inductive (inductive effect), and a smaller R is more π -electron donative (resonance effect). Among the electron-withdrawing substituted iridium(III) complexes, $-\text{CN}$ substituent has the highest F value of 0.51 and hence **Ir3** exhibits oxidation potential of -1.16 V, which is 270 mV smaller than $-\text{CF}_3$ substituted iridium complex **Ir2** having a reduction potential of -1.43 V ($F = 0.38$). However, the reduction potential of **Ir1** is much lower than anticipated (-0.94 V vs Fc^+/Fc) as per the Swain-Lupton constant. This can be attributed to the reduction of the $-\text{CHO}$ group instead of the cyclometalated ligand as usually found in aromatic aldehydes.¹⁰⁰ This finding correlates well with the localization of mostly $-\text{CHO}$ group in the LUMO orbitals of **Ir1** (Fig. 3).

Table 5 Solution state photophysical properties of Ir^{3+} complexes **Ir1 – Ir5**

Complex	Absorption λ_{max} (nm) ($\epsilon \times 10^3 \text{ M}^{-1} \text{ cm}^{-1}$)	Emission at 298 K in CH_2Cl_2 Solution				Emission 77 K ^f	λ_{max} (nm)
		λ_{max} ^b (nm)	Φ_{PL} ^c	τ_{PL} (μs)	k_r ^d (10^5 s^{-1})		
Ir1	233 (20.0), 394 (3.0), 482 (0.2)	540	0.79	1.94	4.07	1.08	511
Ir2	256 (26.0), 378 (4.0), 452 (0.4)	468, 492	0.88	2.36	3.72	0.50	466
Ir3	233 (19.0), 391 (3.0), 464 (0.4)	508	0.90	2.14	4.20	0.46	485
Ir4	252 (34.0), 356 (4.0), 430 (0.1)	436, 464	0.58	1.13	5.13	3.71	434
Ir5	257 (35.0), 343 (9.0), 420 (0.6)	520	0.14	0.31	4.51	27.74	476

^a Absorption spectrum was measured in dichloromethane solution; $[\text{M}] = 5.0 \times 10^{-5}$. ^b Emission spectrum was measured in degassed dichloromethane; $[\text{M}] = 5.0 \times 10^{-5}$, $\lambda_{\text{exc}} = 360$ nm. ^c Phosphorescence quantum efficiency measured in degassed CH_2Cl_2 by relative method by using Quinine sulphate monohydrate ($\Phi_{\text{PL}} = 0.54$) and $\text{Ir}(\text{ppy})_3$ ($\Phi_{\text{PL}} = 0.98$) as standards, respectively for blue and green emitting complexes. ^{d,e} Radiative as well as non-radiative rate constants were deduced by the Φ_{PL} of solution state and τ_{obs} according to two equations: $k_r = \Phi_{\text{PL}}/\tau_{\text{obs}}$, $k_{\text{nr}} = (1 - \Phi_{\text{PL}})/\tau_{\text{obs}}$. ^f Emission spectrum was measured in freeze dichloromethane at 77K; $[\text{M}] = 5.0 \times 10^{-5}$, $\lambda_{\text{exc}} = 360$ nm.

Electronic spectroscopy.

The UV-Vis absorption spectra of iridium(III) compounds **Ir1-Ir5** recorded in degassed dichloromethane ($c = 5 \times 10^{-5}$ M) solution at room temperature are displayed in Fig. 5, and the corresponding electronic absorption data are summarized in Table 5. The absorption of these complexes show intense bands with extinction coefficients in the order of $10^4 \text{ M}^{-1} \text{ cm}^{-1}$ in the 230-300 nm range, which were assigned to the spin-allowed intra-ligand ^1LC ($^1\pi \rightarrow \pi^*$) transition of cyclometalated 2',6'-difluoro-2,3'-bipyridine derivatives and picolinate ligands. The broad band around 370-400 nm can be assigned to spin allowed metal-ligand charge-transfer ($^1\text{MLCT}$) bands with extinction coefficients in the order of $10^3 \text{ M}^{-1} \text{ cm}^{-1}$. In addition, the spin-forbidden $^3\text{MLCT}$ transition bands noted around 420-464 nm indicate an efficient spin-orbit coupling, which is a prerequisite for phosphorescent emission (inset of Fig. 5). These assignments were supported by theoretical calculations (as can be seen from Table S8 ESI[†]). The nature of substituents on the 4' position on the pyridyl moiety of the cyclometalated ligand has significant effects on the extinction coefficient values of the intra-ligand ($\pi \rightarrow \pi^*$) transition band. However, no influence on the location of intra-ligand transition has been observed. The electron-donating group substituted iridium(III) complexes (**Ir4 - Ir5**) exhibit extinction coefficients in the range $34600 - 35000 \text{ M}^{-1} \text{ cm}^{-1}$ for the $\pi \rightarrow \pi^*$ transition. On the other hand, low extinction coefficients $19063 - 26068 \text{ M}^{-1} \text{ cm}^{-1}$ are noted in

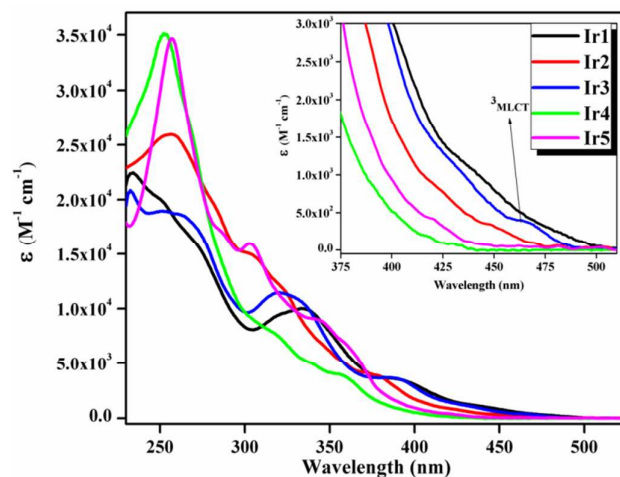


Fig. 5 UV-vis absorption spectra of complexes **Ir1-Ir5** in dichloromethane ($c = 5 \times 10^{-5}$ M) at 298 K (inset: magnified absorption at 300- 500 nm region).

the case of electron-withdrawing group containing complexes (**Ir1-Ir3**). Though the substituents have small influence on the extinction coefficient at $^1\text{MLCT}$ transition, there are significant differences on the location of these transitions. The substitution of electron-donating groups ($-\text{OMe}$ and $-\text{NMe}_2$) in complexes **Ir4-Ir5** shows a blue shifted $^1\text{MLCT}$ absorption bands around 356 and 343 nm, respectively, as compared to electron-withdrawing groups substituted complexes **Ir1-Ir3** (381-394 nm).

Solution state emission properties.

Fig. 6 shows normalized emission spectra of the investigated iridium(III) complexes **Ir1–Ir5** recorded in degassed dichloromethane solution ($c = 5.0 \times 10^{-5}$ M) at 298 K. The pertaining photophysical data are summarized in Table 5. The strong electron-withdrawing group substituted (–CN) iridium(III) complex (**Ir3**) displays a broad and bright green phosphorescence (450 to 700 nm; $\lambda_{\text{max}} = 506$ nm) at room temperature in dichloromethane solution with an excellent quantum efficiency of 0.90, which is comparable to that of standard green emitter Ir(ppy)₃ ($\Phi_{\text{PL}} = 0.98$).¹⁰¹ The broad emission band exhibited by the **Ir3** without the vibronic structure indicates that phosphorescence is originating from the ³MLCT transition state. On the other hand, iridium(III) complex (**Ir2**) containing less electron-withdrawing –CF₃ group ($\text{C}_{\text{OP}} = 0.54$) exhibits intense sky-blue phosphorescence in the region 468–492 nm with a promising quantum efficiency ($\Phi_{\text{PL}} = 0.88$). It is interesting to note that the observed quantum efficiency of **Ir2** is very much comparable to that of commercial sky-blue emitter Irpic ($\Phi_{\text{PL}} = 0.83$).^{102,103} The vibronic structure of the emission bands in **Ir2** indicates a certain degree of mixing between the ligand centered ³LC and ³MLCT state. Surprisingly, a weak electron-withdrawing –CHO group ($\text{C}_{\text{OP}} = 0.42$) substituted iridium(III) complex (**Ir1**) shows a broad emission profile in the range 470–700 nm ($\lambda_{\text{max}} = 540$ nm) with a quantum yield of 0.79. In general, the substitution of electron-withdrawing groups on the C4' position on the pyridyl moiety red shifted the emission profiles of **Ir1–Ir3** as compared to unsubstituted iridium(III) complex (dfppy)₂Irpic.⁷⁶ Our DFT studies (see above) indicate that the picolinate moiety is essentially acts as an ancillary ligand in **Ir1–Ir3** and the emission properties are mainly of ³MLCT/³LC nature, involving iridium d-orbitals and $\pi\text{-}\pi^*$ orbitals of the electron-withdrawing substituted 2',6'-difluoro-2,3'-bipyridine cyclometalated units. It is well documented that acceptor groups are expected to stabilize the LUMO orbital that is involved by pulling out electron density.¹⁰⁴ This is in good agreement with the earlier investigations, which indicates that the triplet energy level of picolinate lies at high energy level and is not involved in the electronic transition causing phosphorescence emission.^{61,105} On the other hand, in the electron-donating substituted iridium(III) complexes **Ir4–Ir5**, the LUMO levels are found to be mainly located on the picolinate ligand. Therefore the substitution of –OMe group in **Ir4** has induced marginal effects on the phosphorescence emission. However, the strong electron-donating –NMe₂ substituted iridium(III) complex (**Ir5**) shows a broad emission (420–700 nm; $\lambda_{\text{max}} = 520$ nm) without vibrational features in the spectrum. The observed emission features can be attributed to the localization of the frontier molecular orbital on –NMe₂ substituent, which inevitably leads to HOMO destabilization as evident from the theoretical calculations.

To gain insight into the relaxation dynamics of the investigated iridium(III) complexes **Ir1–Ir5**, the phosphorescent lifetimes (τ) in dichloromethane solutions were measured at 298 K (Fig. S45

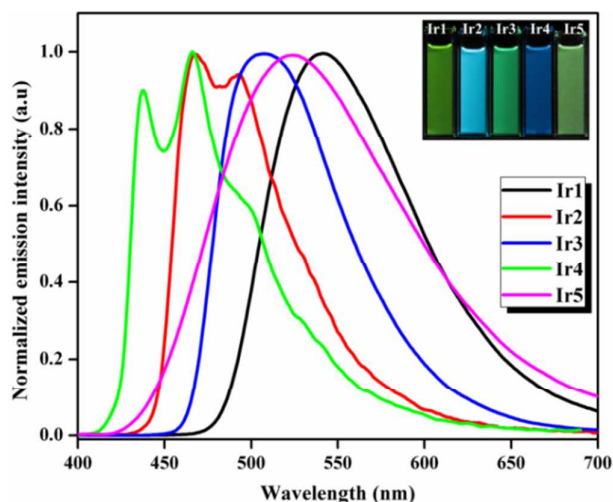


Fig. 6 Emission spectra of complexes **Ir1–Ir5** in dichloromethane ($c = 5 \times 10^{-5}$ M) at 298 K; inset: emission photographs of **Ir1–Ir5** in solution.

ESI[†]). All the complexes showed single exponential decay profiles with lifetimes in the range of 0.31 – 2.36 μs , which are indicative of the phosphorescent origin. The excited state lifetime values, radiative and non-radiative decay rates of the iridium(III) complexes are depicted in Table 5. It is noteworthy to mention that the electron-donating group (–OMe) substituted iridium(III) complex **Ir4** exhibits moderately lower quantum efficiency ($\Phi_{\text{PL}} = 0.58$) when compared to (dfppy)₂Irpic [$\Phi_{\text{PL}} = 0.90$]. This can be explained on the basis of destabilization of LUMO, which will probably decreases the separation of ³MC d-d* state and the designated ³MLCT or ³LC emissive states, consequently intensifies the deactivation pathways. Conversely, poor quantum efficiency is observed in the case of iridium(III) complex **Ir5** due to large vibrational decay pathways ($k_{\text{nr}} = 27.7 \times 10^5 \text{ s}^{-1}$) associated with the –NMe₂ group. At the same time high quantum yields have been noted for complexes **Ir1–Ir3** which are substituted with electron-withdrawing groups. This can be related to the stabilization of LUMO orbitals substituted with electron-withdrawing groups leading to increase the separation of ³MC d-d* state and the designated ³MLCT or ³LC emissive states, and which in turn reduces the deactivation pathways.⁷⁰ This is also in good agreement with the observed low non-radiative decay rates in these complexes ($k_{\text{nr}} = 0.46 – 1.08 \times 10^5 \text{ s}^{-1}$).

It is well known that a minimal difference between the singlet (S_1) and triplet (T_1) splitting energy ($\Delta E_{S_1-T_1}$) is favorable for enhancing the intersystem crossing (ISC) efficiency, which in turn leading to an increased radiative rate constant (k_r).¹⁰⁶ Therefore, it would be informative to obtain further insights into the evolution of k_r by concentrating on singlet–triplet energy differences for these complexes. Thus, a small $\Delta E_{S_1-T_1}$ (Table S9 ESI[†]) and high k_r values (Table 5) noted for **Ir1–Ir3** clearly supports the observed high quantum efficiencies and lifetime values in these compounds. On the other hand, the high $\Delta E_{S_1-T_1}$ values diminish the ISC efficiency in **Ir4** and **Ir5**, which in turn responsible for exhibiting the poor quantum efficiencies and lifetime values in these complexes.

In order to understand the changes in the geometry structures of these complexes upon excitation, the geometry parameters of the complexes in the lowest-lying triplet states (T_1) are calculated (Table S6 ESI[†]). The Ir-N1 (N1: picolinate ligand) bonds are elongated in **Ir4** and **Ir5**, which suggests the larger involvement of the ancillary ligand in the T_1 state rather than from the cyclometalated ligand. Moreover, the elongated distances are responsible for the increase of metal-centered (3MC) non-radiative decay rates that accounts for the less quantum efficiency observed in these complexes. In contrast, the Ir-N1 bonds are not elongated in **Ir1–Ir3** which indicates the ancillary ligand participation in the emissive excited state is minimal. Further the shortening of bond distances (Ir-N2 and Ir-N3) are noted in **Ir1–Ir3**, which suggests that larger involvement of cyclometalating ligand in the T_1 state rather than from the ancillary ligand. Moreover, the shortened distances are helpful to decrease the metal-centered (MC) non-radiative decay that accounts for the higher efficiency in these complexes.

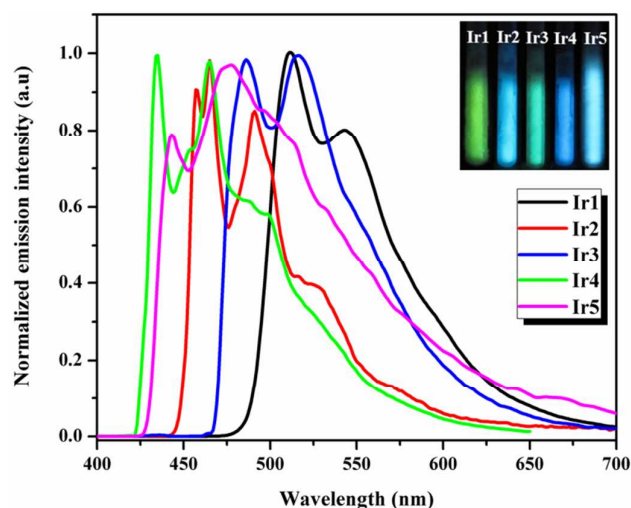


Fig. 7 Emission spectra of complexes **Ir1–Ir5** in freeze dichloromethane ($c = 5 \times 10^{-5}$ M) at 77 K; inset: emission photographs of **Ir1–Ir5** in freeze dichloromethane.

Emission properties in freeze solvent matrix.

It is clear from the emission spectra at 77K depicted in Fig. 7 that all the complexes display vibrational progressions. The peak emissions ($E_{em(0-0)}$) are blue shifted by 44, 29 and 23 nm for **Ir5**, **Ir1** and **Ir3**, respectively, compared to their room temperature peak emissions. This can be attributed to the rigidochromic effect associated with the complexes having greater MLCT character of the emitting state.¹⁰⁷ However, a moderate blue shift (1–4 nm) has been noted in complexes **Ir2** and **Ir4**, indicating the domination of LC character in the excited state.¹⁰⁸ The Full Width Half Maximum (FWHM, $\Delta\nu_{1/2}$) values (Table 6) of the resolved highest energy vibronic bands of **Ir1–Ir5** are 2487, 2326, 3208, 3454 and 4672 cm^{-1} , respectively. The large FWHM value of **Ir5** indicates the highest reorganizational energy in the corresponding excited state. The energy difference of first two emission peaks ($\hbar\omega_M$ value) of these complexes lie in the range of 1457–1609 cm^{-1}

indicating that the dominant vibrational mode associated with the excited distortion can be ascribed to the aromatic in-plane and out-of-plane ring stretching and bending vibrations (ring breathing modes).^{109–116} The degree of the vibrational non-radiative decay can be estimated by the Huang–Rhys factor (S_M). The S_M values of complexes **Ir1–Ir5** are found to be 0.85, 0.99, 1.08, 1.03 and 1.36, respectively (Table 6).

Table 6 Excited state properties of Ir^{3+} complexes **Ir1–Ir5**

Complex	^a $E_{em(0-0)}$ (nm)	^b $\Delta\nu_{1/2}$ (cm^{-1})	^c $\hbar\omega_M$ (cm^{-1})	^d S_M
Ir1	511	2487	1153	0.85
Ir2	457	2326	1562	0.99
Ir3	486	3208	1197	1.08
Ir4	435	3454	1437	1.03
Ir5	443	4672	1609	0.36

^aObtained from the peak emission wavelength in dichloromethane at 77K. ^bFull width half maximum for the (0-0) band obtained from the emission spectra at 77K. ^cFrom the energy difference of first two emission peaks at 77K. ^dThe Huang–Rhys factor, S_M was estimated from the peak heights and energies of the first two peaks of the emission spectra at 77 K [$S_M = (I_{0,1}/I_{0,0}) (\bar{\nu}_{0,0}/\bar{\nu}_{0,1})$].

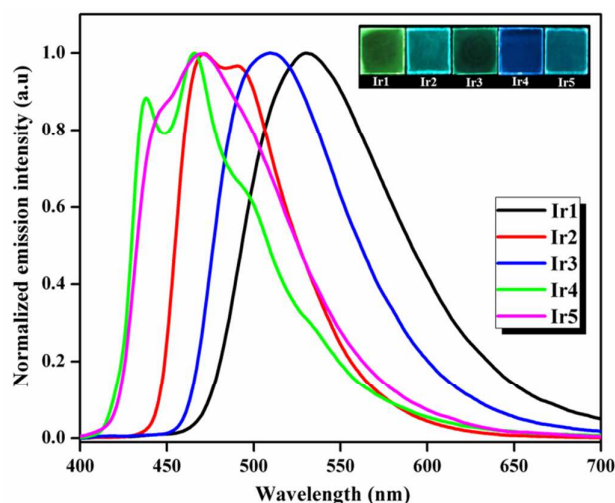


Fig. 8 Emission spectra of complexes **Ir1–Ir5** in 5 wt % doped PMMA film; inset: emission photographs of **Ir1–Ir5** in spin coated PMMA film.

The larger the S_M value, the stronger the coupling between the dominant ligand-localized vibrations in the excited and ground states.^{117, 118} Thus a large Huang–Rhys factor leads to increased vibrational non-radiative decay and as a result small Φ_{PL} in **Ir5**.

Emission properties in PMMA polymer matrix.

Fig. 8 gives the normalized emission spectra of 5 wt % of **Ir1–Ir5** doped in a poly(methyl methacrylate) (PMMA) polymer film at ambient temperature. In the spin coated thin films, complexes **Ir2**, **Ir3** and **Ir4** exhibited virtually identical emission profiles similar to those observed in the corresponding fluid state, which indicate that there is little intermolecular interaction in the amorphous state.⁷⁶ However, **Ir1** and **Ir5** exhibited strong emissions with a blue shift (10 nm for **Ir1** and 50 nm for **Ir5**) with less resolved emission compared to those observed in the corresponding fluid state. The photoluminescence quantum efficiencies are found to be 0.67,

0.84, 0.98, 0.94 and 0.40 for complexes **Ir1**–**Ir5**, respectively, for the doped PMMA films (Table 7).

Table 7 Photophysical properties of Ir³⁺ complexes **Ir1** – **Ir5** in PMMA polymer film

Complex	Emission at 298 K in 5 wt% doped PMMA film				
	λ_{max}^a (nm)	Φ_{Pl}^b	τ_{Pl}^c (μs)	k_r^c (10^5 s^{-1})	k_{nr}^d (10^5 s^{-1})
Ir1	530	0.67	2.14	3.13	1.54
Ir2	470, 491	0.84	1.91	4.39	0.83
Ir3	508	0.98	2.15	4.55	0.09
Ir4	437, 465	0.92	1.85	4.97	0.43
Ir5	470	0.40	1.11	3.60	5.40

^aEmission spectrum was measured in 5wt% doped PMMA film, $\lambda_{\text{exc}} = 360 \text{ nm}$.

^bQuantum efficiency measured by absolute method using integrating sphere.

^{c,d}Radiative as well as non-radiative rate constants were deduced by the Φ_{Pl} of solid state and τ_{obs} according to two equations: $k_r = \Phi_{\text{Pl}}/\tau_{\text{obs}}$, $k_{\text{nr}} = (1 - \Phi_{\text{Pl}})/\tau_{\text{obs}}$.

In general, all the compounds exhibited higher quantum efficiencies in PMMA thin films as compared to solution state due to the suppression of non-radiative pathways in the rigid polymer. The transient phosphorescence lifetimes for complex **Ir1**–**Ir5** are in the range 1.11–2.15 μs (Table 7 and Fig. S46 ESI†). The observed k_{nr} values of the iridium(III) complexes in the current study can be correlated to the nature of the substituent on the cyclometalated ligands. Among the substituents investigated, in general the electron-withdrawing substituted iridium(III) complexes have low k_{nr} values and hence exhibit high quantum efficiency. Conversely, electron-donating group (-NMe₂) substituted iridium(III) complex (**Ir5**) has the highest k_{nr} value, which displays lowest quantum efficiency due to the distortional vibrations of the dimethyl amino group causing a great deal of non-radiative depopulation of the excited state.¹¹⁹ However, the –OMe substituted **Ir4** shows promising quantum efficiency which is having low k_{nr} and highest k_r among the series.

Electroluminescent properties.

To evaluate the performance of the new Ir(III) compounds in PhOLEDs, we prepared a series of devices using a multi-layered structure with CBP (4,4'-Bis(*N*-carbazolyl)-1,1'-biphenyl) as the host. The typical structure of the multi-layered devices is ITO (120 nm) / F₄-TCNQ (2.5 nm) / α -NPD (45 nm) / Emissive layer (30 nm)/BCP (6 nm)/Alq₃ (30 nm)/LiF (1 nm)/Al (150 nm), as shown in Fig. 9. Fig. 10 depicts the EL spectra of OLEDs fabricated using 5 wt % **Ir2**, **Ir3** and **Ir4** doped CBP. 5 wt % **Ir2** doped in CBP showed EL spectrum with a dominant peak at 480 nm and a shoulder peak at 520 nm owing to triplet exciton relaxation. EL spectra of **Ir2** is found to differ from its PL spectra mainly the peak observed nearly at 500 nm has reduced in intensity in the EL spectra and both peaks has been red shifted in EL. Device with 5 wt % **Ir3** doped CBP as emissive layer has peak at 530 nm and the shape of EL spectra nearly resembles to the PL spectra. EL spectrum of 5 wt % **Ir4** doped CBP is constituted of three peaks at 460, 490 and 540 nm, respectively. CIE co-ordinates measured for these devices are listed in Table 8 and also depicted inside the CIE diagram in Fig. 10. It is evident from the figure that **Ir2** emits in bluish region, **Ir3** in green while **Ir4** in blue region of visible spectrum as also

observed from the PL results. It is interesting note that there is no residual emission from the host CBP for each device, which means that the energy and/or charge transfer from the host exciton to the phosphor is complete upon electrical excitation.

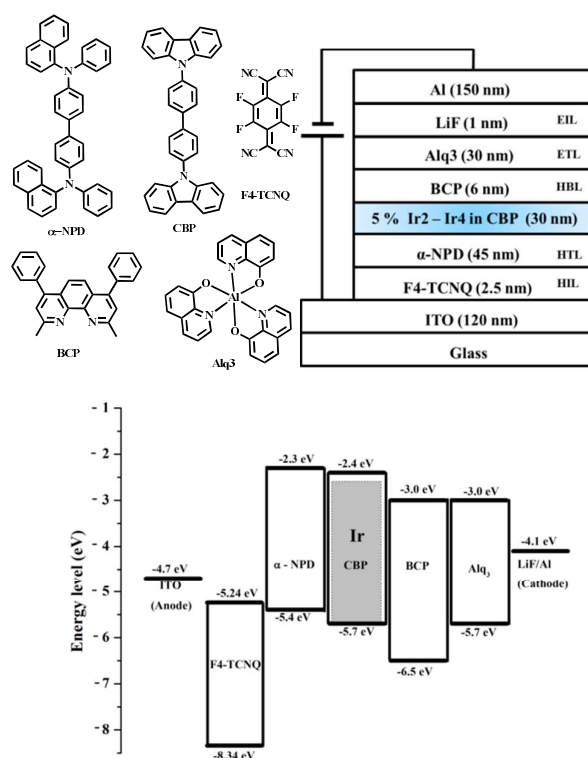


Fig. 9 Schematic EL device structure (right top), the chemical formulas of materials used for the device preparation (left top) and energy level diagram of the device with Ir(III) compounds (**Ir2**–**Ir4**) as dopants (bottom).

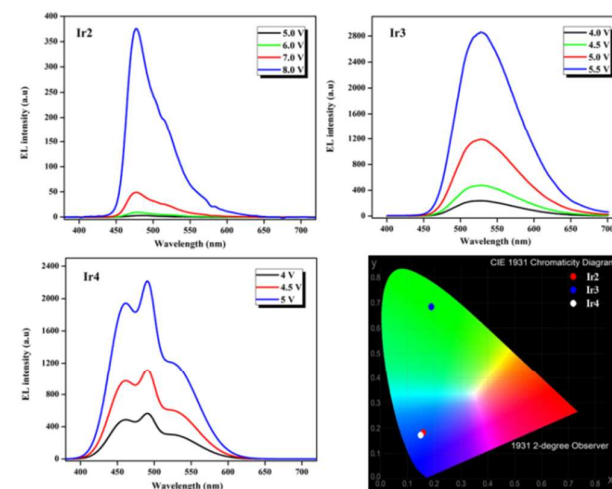


Fig. 10 Electroluminescence (EL) plots for compounds **Ir2**–**Ir4** and CIE 1931 chromaticity diagram for the device with Ir(III) compounds (**Ir2**–**Ir4**) as dopants (right bottom).

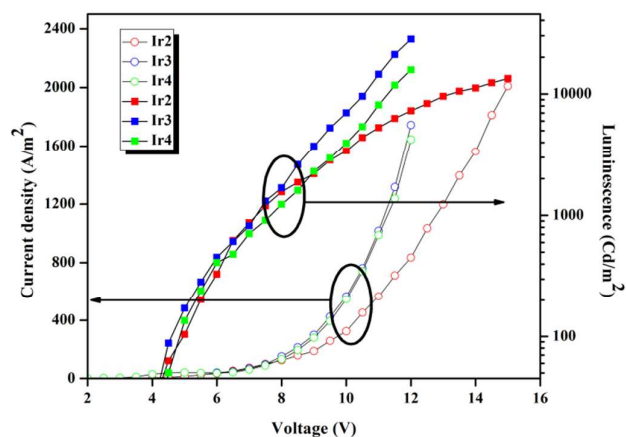


Fig. 11 Current density–voltage–luminescence (J–V–L) characteristics of Ir2–Ir4 as phosphorescent dopants.

Table 8 EL performance data of the Ir2, Ir3 and Ir4 as phosphorescent dopant in CBP

Device	V_{on} (V)	L_{max} (cd/m^2)	η_c (Cd/A)	η_p (lm/W)	EQE (max)	$CIE_{(x,y)}$
Ir2	3.5	13,400	12.6	5.3	3.2 %	(0.16, 0.18)
Ir3	3.5	28,200	14.7	7.6	2.1 %	(0.19, 0.68)
Ir4	3.5	33,180	11.6	5.8	4.7 %	(0.15, 0.17)

Fig. 11 shows the J–V–L characteristics of these devices and the efficiency parameters are listed in Table 8. All devices were found to possess low turn-on voltage (3.5 V) corresponding to a luminous intensity of 10 Cd/m^2 . OLED with 5 wt % Ir2 doped CBP as emissive layer showed a maximum luminescence of about 15000 Cd/m^2 with peak current and power efficiency of 12.6 Cd/A and 5.3 lm/W , respectively. The peak efficiency for OLEDs with 5 wt % Ir3 doped CBP and 5 wt % Ir4 doped CBP were found to be 14.5 Cd/A , 7.6 lm/W and 11.6 Cd/A , 5.76 lm/W , respectively. EL results indicate that the synthesized materials can be used as efficient phosphorescent dopants.

Conclusions

In conclusion, a series of bis(2',6'-difluoro-2,3'-bipyridinato-N,C4')iridium(picolate) complexes [(dfppy)₂Ir(pic): Ir1–Ir5] with different electron-withdrawing (–CHO, –CF₃ and –CN) and electron-donating substituents (–OMe and –NMe₂) on the 4' position on the pyridyl moiety of the 2',6'-difluoro-2,3'-bipyridine ligands has been synthesized, well characterized and investigated their photophysical properties. The results demonstrated that the phosphorescence emission colour of the iridium complexes and quantum efficiencies are influenced by the electron-withdrawing or electron-donating feature of the substituent. The electron-withdrawing groups (–CHO, –CF₃, –CN) substituted iridium(III) complexes Ir1–Ir3 display intense yellowish green, sky-blue and green emissions, respectively, at room temperature in both solution and in thin-film with excellent quantum efficiencies (Φ_{PL} = 0.79–0.90 in solution and 0.67 to 0.98 in thin film). The iridium(III) complex bearing electron-donating group (–OMe) shows pure and intense blue emission with promising quantum efficiency in solution (Φ_{PL} =

0.58) and in thin-film (Φ_{PL} = 0.92). Conversely, –NMe₂ substituted iridium(III) complex (Ir5) exhibits a broad emission in the green region with poor quantum efficiency (Φ_{PL} = 0.14 in solution; 0.40 in thin-film). DFT calculations disclose that the picolate moiety is essentially acts as an ancillary ligand in Ir1–Ir3 and the emission properties are mainly manifested by ³MLCT/³LC, involving iridium d-orbitals and π - π^* orbitals of the electron-withdrawing substituted 2',6'-difluoro-2,3'-bipyridine cyclometalated units. On the other hand, in the electron-donating substituted iridium(III) complexes Ir4–Ir5, the LUMO levels are found to be mainly localized on the picolate ligand. Thus the phosphorescence of Ir4–Ir5 may be resulted from mixed ³LC and ³MLCT transitions. Most importantly, the –OMe, –CF₃ and –CN substituted iridium(III) complexes display excellent emissions in the blue and green regions with high quantum efficiencies. The combination of smaller $\Delta E_{S_1-T_1}$ and higher contribution of MLCT in the emission process result in the higher quantum yields and excited state lifetimes in Ir1–Ir3 compounds. Finally, fabrication of complex Ir4 successfully achieves nearly deep-blue OLEDs, showing a bright blue emission with CIE of (0.15, 0.17), power efficiency of 5.76 $lm W^{-1}$, and an EQE as high as 4.7% with maximum luminance of 33,180 cdm^{-2} . The results clearly demonstrate that the newly designed iridium(III) complexes exhibit excellent thermal and morphological stabilities and electroluminescent properties. Hence these complexes may find potential applications in PhOLEDs.

Acknowledgements

The authors acknowledge financial support from the CSIR, New Delhi, India [CSIR-TAPSUN project, SSL (OLEDs), NWP-55]. K. S. B thanks CSIR, New Delhi for the award of Senior Research Fellowship.

Notes and references

- H. Yersin, *Highly Efficient OLEDs with Phosphorescent Materials*, Wiley-VCH, Weinheim, Germany 2008.
- S. M. Chen, G. P. Tan, W. Y. Wong and H. S. Kwok, *Adv. Funct. Mater.*, 2011, **21**, 3785–3793.
- S. C. Lo, R. N. Bera, R. E. Harding, P. L. Burn and I. D. W. Samuel, *Adv. Funct. Mater.*, 2008, **18**, 3080–3090.
- Z. Q. Chen, Z. Q. Bian and C. H. Huang, *Adv. Mater.*, 2010, **22**, 1534–1539.
- E. Holder, B. M. W. Langeveld and U. S. Schubert, *Adv. Mater.*, 2005, **17**, 1109–1121.
- D. M. Kang, J. W. Kang, J. W. Park, S. O. Jung, S. H. Lee, H. D. Park, Y. H. Kim, S. C. Shin, J. J. Kim and S. K. Kwon, *Adv. Mater.*, 2008, **20**, 2003–2008.
- L. X. Xiao, Z. J. Chen, B. Qu, J. X. Luo, S. Kong, Q. H. Gong and J. J. Kido, *Adv. Mater.*, 2011, **23**, 926–952.
- C. Adachi, R. C. Kwong, P. Djurovich, V. Adamovich, M. A. Baldo, M. E. Thompson and S. R. Forrest, *Appl. Phys. Lett.*, 2001, **79**, 2082–2084.
- P. T. Chou and Y. Chi, *Chem. Eur. J.*, 2007, **13**, 380–395.

- 10 C. H. Hsieh, F. I. Wu, C. H. Fan, M. J. Huang, K. Y. Lu, P. Y. Chou, Y. H. O. Yang, S. H. Wu, I. C. Chen, S. H. Chou, K. T. Wong and C. H. Cheng, *Chem. Eur. J.*, 2011, **17**, 9180-9187.
- 11 Y. Chi and P. T. Chou, *Chem. Soc. Rev.*, 2007, **36**, 1421-1431.
- 12 Y. N. Hong, J. W. Y. Lam and B. Z. Tang, *Chem. Soc. Rev.*, 2011, **40**, 5361-5388.
- 13 J. A. G. Williams, A. J. Wilkinson and V. L. Whittle, *Dalton Trans.*, 2008, 2081-2099.
- 14 Y. Y. Chang, J. Y. Hung, Y. Chi, J. P. Chyn, M. W. Chung, C. L. Lin, P. T. Chou, G. H. Lee, C. H. Chang and W. C. Lin, *Inorg. Chem.*, 2011, **50**, 5075-5084.
- 15 B. S. Du, C. H. Lin, Y. Chi, J. Y. Hung, M. W. Chung, T. Y. Lin, G. H. Lee, K. T. Wong, P. T. Chou, W. Y. Hung and H. C. Chiu, *Inorg. Chem.*, 2010, **49**, 8713-8723.
- 16 V. K. Rai, M. Nishiura, M. Takimoto, S. S. Zhao, Y. Liu and Z. M. Hou, *Inorg. Chem.*, 2012, **51**, 822-835.
- 17 X. F. Ren, M. E. Kondakova, D. J. Giesen, M. Rajeswaran, M. Madaras and W. C. Lenhart, *Inorg. Chem.*, 2010, **49**, 1301-1303.
- 18 D. Schneidenbach, S. Ammermann, M. Debeaux, A. Freund, M. Zollner, C. Daniliuc, P. G. Jones, W. Kowalsky and H. H. Johannes, *Inorg. Chem.*, 2010, **49**, 397-406.
- 19 C. Adachi, M. A. Baldo, M. E. Thompson and S. R. Forrest, *J. Appl. Phys.*, 2001, **90**, 5048-5051.
- 20 W. Y. Wong and C. L. Ho, *J. Mater. Chem.*, 2009, **19**, 4457-4482.
- 21 J. M. Fernandez-Hernandez, C. H. Yang, J. I. Beltran, V. Lemaure, F. Polo, R. Frohlich, J. Cornil and L. De Cola, *J. Am. Chem. Soc.*, 2011, **133**, 10543-10558.
- 22 M. K. Nazeeruddin, R. Humphry-Baker, D. Berner, S. Rivier, L. Zuppiroli and M. Graetzel, *J. Am. Chem. Soc.*, 2003, **125**, 8790-8797.
- 23 M. A. Baldo, D. F. O'Brien, Y. You, A. Shoustikov, S. Sibley, M. E. Thompson and S. R. Forrest, *Nature*, 1998, **395**, 151-154.
- 24 C. L. Ho and W. Y. Wong, *New J. Chem.*, 2013, **37**, 1665-1683.
- 25 Y. J. Pu, N. Iguchi, N. Aizawa, H. Sasabe, K. Nakayama and J. Kido, *Org. Electron.*, 2011, **12**, 2103-2110.
- 26 M. A. Baldo, C. Adachi and S. R. Forrest, *Phys. Rev. B.*, 2000, **62**, 10967-10977.
- 27 M. A. Baldo, S. Lamansky, P. E. Burrows, M. E. Thompson and S. R. Forrest, *Appl. Phys. Lett.*, 1999, **75**, 4-6.
- 28 S. Lamansky, P. Djurovich, D. Murphy, F. Abdel-Razzaq, H. E. Lee, C. Adachi, P. E. Burrows, S. R. Forrest and M. E. Thompson, *J. Am. Chem. Soc.*, 2001, **123**, 4304-4312.
- 29 Z. W. Liu, M. Guan, Z. Q. Bian, D. B. Nie, Z. L. Gong, Z. B. Li and C. H. Huang, *Adv. Funct. Mater.*, 2006, **16**, 1441-1448.
- 30 W. Y. Wong, G. J. Zhou, X. M. Yu, H. S. Kwok and B. Z. Tang, *Adv. Funct. Mater.*, 2006, **16**, 838-846.
- 31 C. H. Yang, W. L. Su, K. H. Fang, S. P. Wang and I. W. Sun, *Organometallics*, 2006, **25**, 4514-4519.
- 32 W. Y. Wong, G. J. Zhou, X. M. Yu, H. S. Kwok and Z. Y. Lin, *Adv. Funct. Mater.*, 2007, **17**, 315-323.
- 33 G. J. Zhou, W. Y. Wong, B. Yao, Z. Y. Xie and L. X. Wang, *Angew. Chem. Int. Ed.*, 2007, **46**, 1149-1151.
- 34 Y. Chi and P. T. Chou, *Chem. Soc. Rev.*, 2010, **39**, 638-655.
- 35 P. S. Wagenknecht and P. C. Ford, *Coord. Chem. Rev.*, 2011, **255**, 591-616.
- 36 D. Tanaka, H. Sasabe, Y. J. Li, S. J. Su, T. Takeda and J. Kido, *Japanese Journal of Applied Physics Part 2-Letters & Express Letters*, 2007, **46**, L10-L12.
- 37 C. H. Yang, Y. M. Cheng, Y. Chi, C. J. Hsu, F. C. Fang, K. T. Wong, P. T. Chou, C. H. Chang, M. H. Tsai and C. C. Wu, *Angew. Chem. Int. Ed.*, 2007, **46**, 2418-2421.
- 38 Y. S. Park, J. W. Kang, D. M. Kang, J. W. Park, Y. H. Kim, S. K. Kwon and J. J. Kim, *Adv. Mater.*, 2008, **20**, 1957-+.
- 39 D. S. Leem, S. O. Jung, S. O. Kim, J. W. Park, J. W. Kim, Y. S. Park, Y. H. Kim, S. K. Kwon and J. J. Kim, *J. Mater. Chem.*, 2009, **19**, 8824-8828.
- 40 M. G. Helander, Z. B. Wang, J. Qiu, M. T. Greiner, D. P. Puzzo, Z. W. Liu and Z. H. Lu, *Science*, 2011, **332**, 944-947.
- 41 S. Y. Kim, W. I. Jeong, C. Mayr, Y. S. Park, K. H. Kim, J. H. Lee, C. K. Moon, W. Brutting and J. J. Kim, *Adv. Funct. Mater.*, 2013, **23**, 3896-3900.
- 42 S. Lee, K. H. Kim, D. Limbach, Y. S. Park and J. J. Kim, *Adv. Funct. Mater.*, 2013, **23**, 4105-4110.
- 43 S. Lee, D. Limbach, K. H. Kim, S. J. Yoo, Y. S. Park and J. J. Kim, *Org. Electron.*, 2013, **14**, 1856-1860.
- 44 Y. S. Park, S. Lee, K. H. Kim, S. Y. Kim, J. H. Lee and J. J. Kim, *Adv. Funct. Mater.*, 2013, **23**, 4914-4920.
- 45 N. G. Park, M. Y. Kwak, B. O. Kim, O. K. Kwon, Y. K. Kim, B. You, T. W. Kim and Y. S. Kim, *Jpn J Appl Phys 1*, 2002, **41**, 1523-1526.
- 46 A. B. Tamayo, B. D. Alleyne, P. I. Djurovich, S. Lamansky, I. Tsyba, N. N. Ho, R. Bau and M. E. Thompson, *J. Am. Chem. Soc.*, 2003, **125**, 7377-7387.
- 47 T. Tsuzuki, N. Shirasawa, T. Suzuki and S. Tokito, *Adv. Mater.*, 2003, **15**, 1455-1458.
- 48 W. Y. Wong, C. L. Ho, Z. Q. Gao, B. X. Mi, C. H. Chen, K. W. Cheah and Z. Y. Lin, *Angew. Chem. Int. Ed.*, 2006, **45**, 7800-7803.
- 49 D. Tanaka, Y. Agata, T. Takeda, S. Watanabe and J. Kido, *Jpn J Appl Phys 2*, 2007, **46**, L117-L119.
- 50 H. H. Chou and C. H. Cheng, *Adv. Mater.*, 2010, **22**, 2468-2477.
- 51 Y. T. Tao, Q. A. Wang, C. L. Yang, C. Zhong, J. G. Qin and D. G. Ma, *Adv. Funct. Mater.*, 2010, **20**, 2923-2929.
- 52 V. V. Grushin, N. Herron, D. D. LeCloux, W. J. Marshall, V. A. Petrov and Y. Wang, *Chem. Commun.*, 2001, 1494-1495.
- 53 P. Coppo, E. A. Plummer and L. De Cola, *Chem. Commun.*, 2004, 1774-1775.
- 54 R. Ragni, E. A. Plummer, K. Brunner, J. W. Hofstraat, F. Babudri, G. M. Farinola, F. Naso and L. De Cola, *J. Mater. Chem.*, 2006, **16**, 1161-1170.
- 55 I. Avilov, P. Minoofar, J. Cornil and L. De Cola, *J. Am. Chem. Soc.*, 2007, **129**, 8247-8258.
- 56 L. L. Wu, C. H. Yang, I. W. Sun, S. Y. Chu, P. C. Kao and H. H. Huang, *Organometallics*, 2007, **26**, 2017-2023.
- 57 H. J. Seo, K. M. Yoo, M. Song, J. S. Park, S. H. Jin, Y. I. Kim and J. J. Kim, *Org. Electron.*, 2010, **11**, 564-572.
- 58 S. Aoki, Y. Matsuo, S. Ogura, H. Ohwada, Y. Hisamatsu, S. Moromizato, M. Shiro and M. Kitamura, *Inorg. Chem.*, 2011, **50**, 806-818.

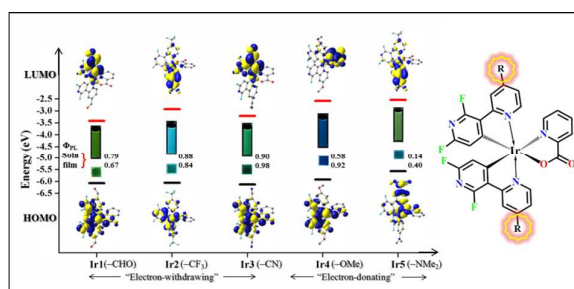
- 59 V. N. Kozhevnikov, K. Dahms and M. R. Bryce, *J. Org. Chem.*, 2011, **76**, 5143-5148.
- 60 M. L. Xu, R. Zhou, G. B. Che, G. Y. Wang, Z. J. Wang and Q. Xiao, *J. Lumin.*, 2011, **131**, 909-914.
- 61 E. Baranoff, B. F. E. Curchod, F. Monti, F. Steimer, G. Accorsi, I. Tavernelli, U. Rothlisberger, R. Scopelliti, M. Gratzel and M. K. Nazeeruddin, *Inorg. Chem.*, 2012, **51**, 799-811.
- 62 C. Fan, Y. H. Li, C. L. Yang, H. B. Wu, J. G. Qin and Y. Cao, *Chem. Mater.*, 2012, **24**, 4581-4587.
- 63 S. Lee, S. O. Kim, H. Shin, H. J. Yun, K. Yang, S. K. Kwon, J. J. Kim and Y. H. Kim, *J. Am. Chem. Soc.*, 2013, **135**, 14321-14328.
- 64 H. Oh, K. M. Park, H. Hwang, S. Oh, J. H. Lee, J. S. Lu, S. N. Wang and Y. Kang, *Organometallics*, 2013, **32**, 6427-6436.
- 65 H. J. Park, J. N. Kim, H. J. Yoo, K. R. Wee, S. O. Kang, D. W. Cho and U. C. Yoon, *J. Org. Chem.*, 2013, **78**, 8054-8064.
- 66 C. Shi, H. B. Sun, Q. B. Jiang, Q. Zhao, J. X. Wang, W. Huang and H. Yan, *Chem. Commun.*, 2013, **49**, 4746-4748.
- 67 Q. L. Xu, C. C. Wang, T. Y. Li, M. Y. Teng, S. Zhang, Y. M. Jing, X. Yang, W. N. Li, C. Lin, Y. X. Zheng, J. L. Zuo and X. Z. You, *Inorg. Chem.*, 2013, **52**, 4916-4925.
- 68 S. Haneder, E. Da Como, J. Feldmann, J. M. Lupton, C. Lennartz, P. Erk, E. Fuchs, O. Molt, I. Munster, C. Schildknecht and G. Wagenblast, *Adv. Mater.*, 2008, **20**, 3325-3328.
- 69 H. Sasabe, T. Chiba, S. J. Su, Y. J. Pu, K. I. Nakayama and J. Kido, *Chem. Commun.*, 2008, 5821-5823.
- 70 P. T. Chou, Y. Chi, M. W. Chung and C. C. Lin, *Coord. Chem. Rev.*, 2011, **255**, 2653-2665.
- 71 T. Karatsu, M. Takahashi, S. Yagai and A. Kitamura, *Inorg. Chem.*, 2013, **52**, 12338-12350.
- 72 R. Meerheim, S. Scholz, S. Olthof, G. Schwartz, S. Reineke, K. Walzer and K. Leo, *J. Appl. Phys.*, 2008, **104**, 014510-014515.
- 73 S. Lee, S.-O. Kim, H. Shin, H.-J. Yun, K. Yang, S.-K. Kwon, J.-J. Kim and Y.-H. Kim, *J. Am. Chem. Soc.*, 2013, **135**, 14321-14328.
- 74 H. S. Fu, Y. M. Cheng, P. T. Chou and Y. Chi, *Mater. Today*, 2011, **14**, 472-479.
- 75 S. J. Lee, K. M. Park, K. Yang and Y. Kang, *Inorg. Chem.*, 2009, **48**, 1030-1037.
- 76 Y. Kang, Y. L. Chang, J. S. Lu, S. B. Ko, Y. L. Rao, M. Varlan, Z. H. Lu and S. N. Wang, *J. Mater. Chem. C* 2013, **1**, 441-450.
- 77 C. H. Yang, M. Mauro, F. Polo, S. Watanabe, I. Muenster, R. Frohlich and L. De Cola, *Chem. Mater.*, 2012, **24**, 3684-3695.
- 78 H. R. Park, D. H. Lim, Y. K. Kim and Y. Ha, *J. Nanosci. Nanotechnol.*, 2012, **12**, 668-673.
- 79 F. Kessler, Y. Watanabe, H. Sasabe, H. Katagiri, M. K. Nazeeruddin, M. Gratzel and J. Kido, *J. Mater. Chem. C*, 2013, **1**, 1070-1075.
- 80 S.-J. Lee, S.-G. Yang, H.-Y. Kim, Y.-K. Kim, S.-H. Hwang, D.-Y. Shin, Y.-R. Do, D.-H. Jung and Suwon-si, *U.S. Patent 2005/0170209 A1*, 2005.
- 81 Z. Mingjie, W. Ping and *WIPO Patent WO/2013/000166*, 2013.
- 82 M. Nonoyama, *Bull. Chem. Soc. Jpn.*, 1974, **47**, 767-769.
- 83 F. O. Garces, K. A. King and R. J. Watts, *Inorg. Chem.*, 1988, **27**, 3464-3471.
- 84 K. S. Bejoymohandas, T. M. George, S. Bhattacharya, S. Natarajan and M. L. P. Reddy, *J. Mater. Chem. C*, 2014, **2**, 515-523.
- 85 CrystalClear 2.1, Rigaku Corporation: Tokyo, Japan.
- 86 J. W. Pflugrath, *Acta. Crystallogr. D*, 1999, **55**, 1718-1725.
- 87 G. M. Sheldrick, *SADABS Siemens Area Detector Absorption Correction Program*, University of Göttingen, Göttingen, Germany, 1994.
- 88 A. M. Brouwer, *Pure Appl. Chem.*, 2011, **83**, 2213-2228.
- 89 K. A. King, P. J. Spellane and R. J. Watts, *J. Am. Chem. Soc.*, 1985, **107**, 1431-1432.
- 90 J. C. de Mello, H. F. Wittmann and R. H. Friend, *Adv. Mater.*, 1997, **9**, 230-232.
- 91 Y. Liu, M. S. Liu and A. K. Y. Jen, *Acta Polym.*, 1999, **50**, 105-108.
- 92 A. D. Becke, *J. Chem. Phys.*, 1993, **98**, 5648-5652.
- 93 C. T. Lee, W. T. Yang and R. G. Parr, *Phys. Rev. B*, 1988, **37**, 785-789.
- 94 S. I. Gorelsky, *SWizard program (version 4.6)*, 2007.
- 95 M. J. Frisch, G. W. Trucks, H. B. Schlegel, G. E. Scuseria, M. A. Robb, J. R. Cheeseman, G. Scalmani, V. Barone, B. Mennucci and G. A. Petersson, *et al. GAUSSIAN 09, Revision A.02*, 2009.
- 96 P. Tyagi, A. Kumar, L. I. Giri, M. K. Dalai, S. Tuli, M. N. Kamalasanan and R. Srivastava, *Opt. Lett.*, 2013, **38**, 3854-3857.
- 97 E. Baranoff, B. F. E. Curchod, J. Frey, R. Scopelliti, F. Kessler, I. Tavernelli, U. Rothlisberger, M. Gratzel and M. K. Nazeeruddin, *Inorg. Chem.*, 2012, **51**, 215-224.
- 98 M. L. Xu, G. B. Che, X. Y. Li and Q. Xiao, *Acta. Crystallogr. E*, 2009, **65**, M28-U379.
- 99 C. Hansch, A. Leo and R. W. Taft, *Chem. Rev.*, 1991, **91**, 165-195.
- 100 R. Udhayan, K. Basheerahmed and K. Srinivasan, *Bull. Electrochem.*, 1988, **4**, 163-165.
- 101 T. Hofbeck and H. Yersin, *Inorg. Chem.*, 2010, **49**, 9290-9299.
- 102 Y. M. You and S. Y. Park, *J. Am. Chem. Soc.*, 2005, **127**, 12438-12439.
- 103 Y. You, K. S. Kim, T. K. Ahn, D. Kim and S. Y. Park, *J Phys Chem C*, 2007, **111**, 4052-4060.
- 104 J. Frey, B. F. E. Curchod, R. Scopelliti, I. Tavernelli, U. Rothlisberger, M. K. Nazeeruddin and E. Baranoff, *Dalton Trans.*, 2014, **43**, 5667-5679.
- 105 S. Lamansky, P. Djurovich, D. Murphy, F. Abdel-Razzaq, R. Kwong, I. Tsyba, M. Bortz, B. Mui, R. Bau and M. E. Thompson, *Inorg. Chem.*, 2001, **40**, 1704-1711.
- 106 J. Li, Q. Zhang, H. He, L. Wang and J. Zhang, *Dalton Trans.*, 2015, **44**, 8577-8589.
- 107 K. P. S. Zononi, B. K. Kariyazaki, A. Ito, M. K. Brennaman, T. J. Meyer and N. Y. M. Iha, *Inorg. Chem.*, 2014, **53**, 4089-4099.

COMMUNICATION

Journal Name

- 108 L. L. Han, D. F. Yang, W. L. Li, B. Chu, Y. R. Chen, Z. S. Su, D. Y. Zhang, F. Yan, S. H. Wu, J. B. Wang, Z. Z. Hu and Z. Q. Zhang, *Appl. Phys. Lett.*, 2009, **94**, 3303-3308.
- 109 N. Nakamoto, *Infrared and Raman Spectra of Inorganic and Coordination Compounds*, Wiley, New York, 3rd edn edn., 1977.
- 110 E. M. Kober, J. V. Caspar, R. S. Lumpkin and T. J. Meyer, *J. Phys. Chem.*, 1986, **90**, 3722-3729.
- 111 D. P. Rillema, C. B. Blanton, R. J. Shaver, D. C. Jackman, M. Boldaji, S. Bundy, L. A. Worl and T. J. Meyer, *Inorg. Chem.*, 1992, **31**, 1600-1606.
- 112 H. Yersin, S. Schutzenmeier, H. Wiedenhofer and A. Vonzelewsky, *J. Phys. Chem.*, 1993, **97**, 13496-13499.
- 113 N. H. Damrauer, T. R. Boussie, M. Devenney and J. K. McCusker, *J. Am. Chem. Soc.*, 1997, **119**, 8253-8268.
- 114 W. Humbs and H. Yersin, *Inorg. Chim. Acta*, 1997, **265**, 139-147.
- 115 H. Yersin, *Proc. SPIE-Int. Soc. Opt. Eng.*, 2004, **5214**, 124-140.
- 116 L. L. Han, D. F. Yang, W. L. Li, B. Chu, Y. R. Chen, Z. S. Su, D. Y. Zhang, F. Yan, S. H. Wu, J. B. Wang, Z. Z. Hu and Z. Q. Zhang, *Appl. Phys. Lett.*, 2009, **94**.
- 117 J. V. Caspar, T.D.Westmoreland, G. H. Allen, P. G. Bradley, T. J. Meyer and W. H. Woodruff, *J. Am. Chem. Soc.*, 1984, **106**, 3492-3501.
- 118 R. J. Watts, *Comments Inorg. Chem.*, 1991, **11**, 303-308.
- 119 Y. Y. Lyu, Y. Byun, O. Kwon, E. Han, W. S. Jeon, R. R. Das and K. Char, *J. Phys. Chem. B*, 2006, **110**, 10303-10314.

Table of contents



Electron-withdrawing and electron-donating groups at pyridyl moiety of the cyclometalated ligand have profound effects on the photophysical properties of bis(2',6'-difluoro-2,3'-bipyridinato-N,C4')iridium(picolate) complexes